Imperial College of London
Department of Physics
Experimental Solid State Physics Group

Luminescent Solar Concentrator with a Fibre Geometry

MSc. Energy Science

Oreane Yasmin Edelenbosch

Supervisor
Dr. Amanda J. Chatten
Imperial College of London

Supervisor
Dr. Wilfried G.J.H.M. van Sark
University of Utrecht

November 2011 - April 2012

Abstract

The potential of a luminescent solar concentrator (LSC) with a fibre geometry to concentrate the sunlight has been explored, by means of a theoretical comparison with the conventional flat plate LSC and by simulating the optical efficiency with the ray tracing programme PVtrace. In addition clear sky diffuse and direct spectra have been modelled for London and their contribution to the photons collected have been compared. It is found that looking at the losses caused by reflection, host absorption and the escape cone in combination with the geometrical concentration G, the fibre is found to be 1.5 times as efficient as the flat plate LSC when 0.1 m^{-1} host absorption, low doping and normal incident light is assumed. The simulation showed that, as the path length for absorbed photons to the edge is long, maximum re-absorption occurs, in fibres of 10 cm length and 1 mm radius. Increasing the length from that point, hardly affects the optical efficiency, while the geometrical concentration increases, resulting in a high concentrating potential. A coated fibre is found to be more efficient than a homogeneous doped fibre, because the trapping efficiency is higher when photons are emitted close to the surface in of a cylindrical LSC.

Acknowledgements

First of all I would like to thank Amanda Chatten, for inviting me to come to London to perform this research at your research group at the Imperial College London. It has been a privilege to work with you. Thank you Martyn Fisher, for assisting me with all the lab work, taking the time to discuss several topics with me and getting started with PVtrace. I wish you the best of luck with your research and hope to work together again sometime. A warm thanks goes to Luca Patrignani for always listening and helping, whether it was to clarify my thoughts or working on together on calculations and simulations. Thanks Wilfried van Sark for supervising me from the University of Utrecht. Last but not least, I would also like to mention my room mates at Imperial College, Roberto, John, Kostas, Emma, Ned, Antonio, Yan, Stephen and Sylvain for making every day interesting.

Contents

Chapter 1

Introduction

The radiation of the sun on the earth in 90[1] minutes contains as much energy as we consume in a whole year. It is an abundant, climate friendly, inexhaustible energy source, available in every country and even more in the countries which are expected to experience high economic and population growth in the coming decades [1]. However, converting the energy of the Sun at a high efficiency and especially in a way that can compete economically with conventional energy sources, remains difficult to achieve.

Photovoltaic (PV) systems, which convert photons in to electrons, has been the fastest growing power technology between 2000 and 2010, in terms of the annual rate of the market share. In absolute terms it still consists less than 1% of the market share, indicating that there is still a lot to win[2]. In the last few years China has become a major solar cell and modules manufacturer, which has lowered the prices of the PV systems. Depending on the remoteness of the area, electricity from PV systems can be competitive with retail power prices[1].

The efficiency of solar cells has steadily increased since research in this field started, and continues to do so. Increasing the solar cell efficiency beyond the Schockley-Queisser limit requires complex devices, that often bring higher costs to produce them. An alternative approach to lower cost per installed capacity is by concentrating the sunlight before reaching the solar cell. Nowadays, devices exits that can concentrate solar light between 300-1000 suns, high concentration photovoltaics (HCPV) and between 2-100 or 100-300 suns, low concentration photovoltaics (LCPV). When concentrating up to 100 suns, the heat flux is still low and no cooling is needed. A luminescent solar concentrator (LSC), consisting of a transparent polymer plate doped with luminescent species, has the ability the concentrate the solar photons in the LCPV range, while down-shifting the energy of the photon. The luminescent species emit absorbed light isotropically, of which

[1] 90 minutes is an estimation and depending one how the calculation is performed the time period can be a bit longer or shorter but here the number mainly demonstrates how powerful the Sun is.

a significant part is trapped within the plate and wave guided to the edges due to total internal reflection (TIR). The area-ratio of the top surface where the photons incident and the edges where they are guided to, result in concentration of the light. As the cost of a transparent polymer plate such as a poly methyl methacrylate (PMMA) plate is low compared to a solar cell, using a LSC in combination with a solar cell can decrease the overall cost of the photovoltaic electricity production[3].
The LSC was invented in 1976 by Weber and Lambe[4]. There has been a high interest in the LSC application and different configurations have been researched using various types of luminescent species. Until now however, LCSs have not become commercially viable, because the optical efficiency remains too low. As a response, McIntosh (2007) has recently proposed a new geometry, the cylindrical LSC, which is estimated to be 1-1.9 times as efficient [4]. This result has evoked questions on the applicability and optimal characteristics of the cylindrical LSC and has opened the door for other geometries as well.

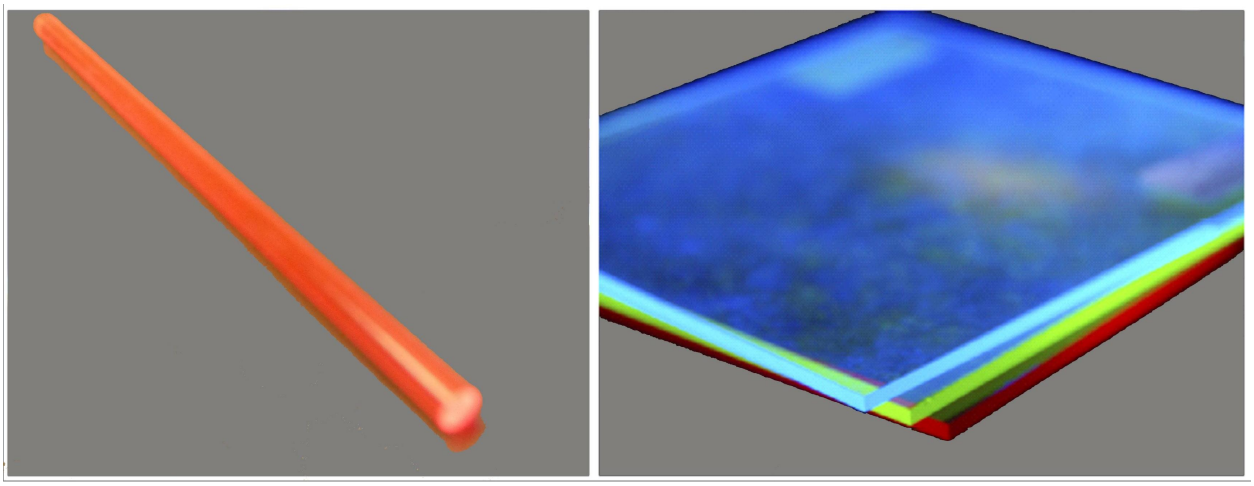

Figure 1.1: Luminescent Solar concentrator with a flat plate [5] and cylindrical geometry.

In the same way that thin plate LSCs have a large area ratio between the incident light surface and the edges, for a cylinder it is characteristic that the longer and thinner it is, the larger this area ratio becomes. Following this reasoning luminescent solar concentrators with a fibre geometry, would have a large concentrating potential. As optical and polymer fibres are already produced at large scale, manufacturing processes of these fibres are well known. The production steps are optimized, resulting in low host material losses and cheap manufacturing cost. At the same time fibres have the advantage that they have a light weight and are flexible.
The key objective of this study is to investigate if fibre based LSCs have the potential to decrease the cost of photovoltaic energy generation. By analysing the interactions between the solar photons and the fibre, while looking at different configurations, a better understanding of the working mechanism of this type of

LSCs will be gained. In addition the aim is to optimize the concentration ability of the fibre LSC as much as possible. By using a Monte Carlo based ray tracing model, the optical efficiency of fibre LSC will be estimated while varying the dimensions of the fibre and the density and location of the luminescent species. Experimental research on fibres with homogeneously dispersed lumogen red dye will be performed to support the results and give insight in the realistic application of fibre LSC.

Luminescent solar concentrators are especially applicable in urban areas because they concentrate the direct as well as the diffuse solar spectrum. Clear sky diffuse and direct spectra for London on a winter and summer day for every hour, will be modelled, to get a better insight on how available light is utilized in the LSC and which fraction of the spectra is wave guided by the LSC. These results, will give us a more detailed insight of the potential of fibre based LSCs to increase the efficiency of photovoltaic electricity production.

In the next chapter the general theory of solar cells and LSCs is explained along with the LSC state of the art. In Chapter 3 a theoretical comparison of the optical efficiency between the LSC flat plate and the LSC fibre is made, based on the losses which are effected by the geometry of the LSC. The following Chapter describes the method and results of the experimental research and the simulations performed. Finally in Chapter 5, the contribution of diffuse and direct spectra to the optical efficiency of the fibre LSC, modelled for London in the winter and in the summer is investigated and compared.

Chapter 2

Theory

Searching for a way to decrease the high cost of photovoltaic energy generation, concentrating the light of the sun is a powerful tool to use. Increasing the photon flux can enlarge the electron collection by the solar cell, resulting in a larger current production, while using the same device. Large areas of expensive solar cells can be replaced by cheaper material concentrators.

The radiant flux coming from the Sun has a spectral distribution from 0.3 to 4 μm. Part of this spectrum is observable in the direction of the Sun, which is called the direct spectrum and part of it is scattered due to molecules, dust, aerosols and clouds, called the diffuse spectrum. The photon flux delivered by the direct and the diffuse spectrum varies throughout the day and the season depending on location, weather and atmospheric composition. In figure 2.1 the global, diffuse and direct spectra in London on a clear sky winter morning is depicted. It is visible that the diffuse spectrum can have a large contribution to the global spectrum.

A conventional solar concentrator concentrates the direct solar spectra, using a parabolic mirror or a Fresnel lens facing the solar beam constantly. In both cases the light is directed to a small receiver, which absorbs the radiation. Luminescent Solar Concentrators (LSC) have a different approach on concentrating light, where the diffuse and the direct spectra are both employed. The diffuse spectrum is more apparent in urban areas, where there are more air pollutants scattering the light and surfaces which reflect the light. In addition, when deploying LSCs, tracking mechanisms are not required [6].

In this chapter first a short description of the solar cell will be given, after which the operating principles of the LSC will be described along with the basic losses and the concentrating potential, concluding with a short overview of the LSC state of the art.

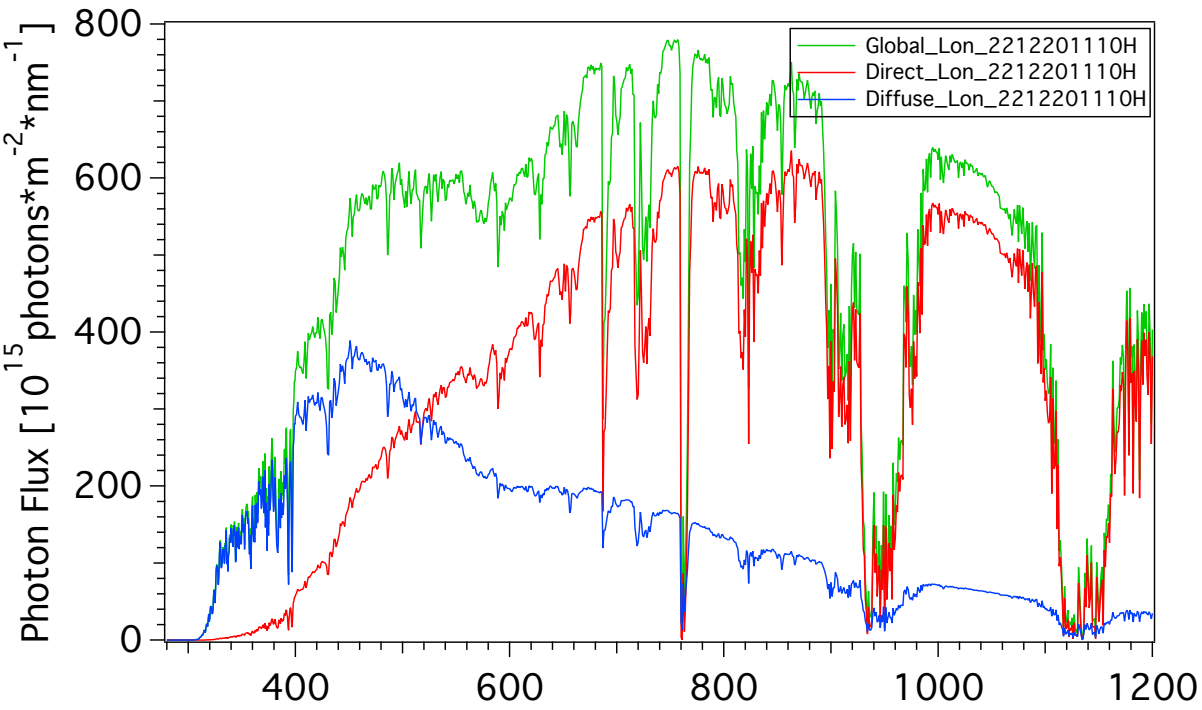

Figure 2.1: Direct, Diffuse and Global Spectrum for London with a clear sky, on the 22nd of December 2011 at 10 AM , simulated by SMARTS (Simple Model of the Atmospheric Radiative Transfer of Sunshine) [7][8]. The weighted average photon energy (APE) for the global spectrum is 1.76 eV, calculated for the 300-1400 nm range, is slightly higher than the 1.714 eV reported for the AM1.5 standard spectrum [9]

2.1 The p-n Junction Solar Cell

The conventional solar cell is a combination of a p-doped semiconductor layer and a n-doped semiconductor layer. An example of such a solar cell is a silicon solar cell doped with boron forming the p-doped layer and with phosphorus to form the n-doped layer. In the n-type region more electrons are present than in the the p-type layer causing electrons to diffuse from the n-type to the p-type layer and in the same way holes to diffuse in opposite direction. Positive ions are left in the n-type region while negative ions are left in the p-type region creating a electric field which counteracts the diffusion and creates a drift of the carriers in the opposite direction. The region where the electric field exists, along with a built in potential, is called the depletion region. When there are no external inputs (light,voltage) present, the drift and the diffusion of the carriers are in equilibrium in the depletion region.

In a semiconductor solar cell a photon, with an energy higher than the band gap energy of the semiconduc-

tor, can be absorbed by transferring its energy to an electron in the valence band and promoting it to the conduction band. The built in potential causes the electrons to drift to the n-side and the holes to drift to the p-side, where they are a majority carrier. The conduction band n-side electrons can flow through an external circuit to recombine with the valence band p-side holes. Power is produced with voltage V which increases with the size of the band gap and a current density J which decreases with the size of the band gap. This ambiguity leads to the Shockley Queisser limit [5].
The photon current density at short circuit can be described by:

$$J_{sc} = q \int QE(E) b_s(E)\, \mathrm{d}E \tag{2.1}$$

where q is the electronic charge, E the energy of the photon, $QE(E)$ the probability for a photon with an energy E to excite an electron that is collected and $\mathrm{b}_s(E)$ the incident spectral photon flux density.
Connecting a load to the device develops a potential difference, creating a dark current flowing in opposite direction to the photo current under an applied voltage or bias V. The asymmetry of the junction is increased inducing more charge separation. The solar cell behaves like a diode in the dark with an ideal current density of:

$$J_{dark}(V) = J_0(E^{qV/(nkT)} - 1) \tag{2.2}$$

where V is the voltage applied, k is the Boltzmann constant, T is the temperature, n is the ideality factor and J_0 is the saturation current. The sum of the photon-generated current density and the dark current density gives the relation between the current density and the voltage applied, which is called the current-voltage characteristic and it can be seen in figure 2.2 for an ideal cell. Given this relationship, the maximum power density produced can be calculated as it is the product of the current density and the voltage [10]. This occurs at the maximum power density point

$$P_m = J_m V_m \tag{2.3}$$

The fill factor FF determines the squareness of the $J(V)$ curve of a solar cell, defined as

$$FF = \frac{V_m J_m}{J_{sc} V_{oc}} \tag{2.4}$$

which relates the maximum power density point to the short-circuit current density and the open-circuit voltage

$$P_m = FF J_{sc} V_{oc}. \tag{2.5}$$

The overall efficiency of the solar cell can therefore be expressed as:

$$\eta_{solarcell} = \frac{P_{out}}{P_{in}} = \frac{FF J_{sc} V_{oc}}{P_{in}}. \tag{2.6}$$

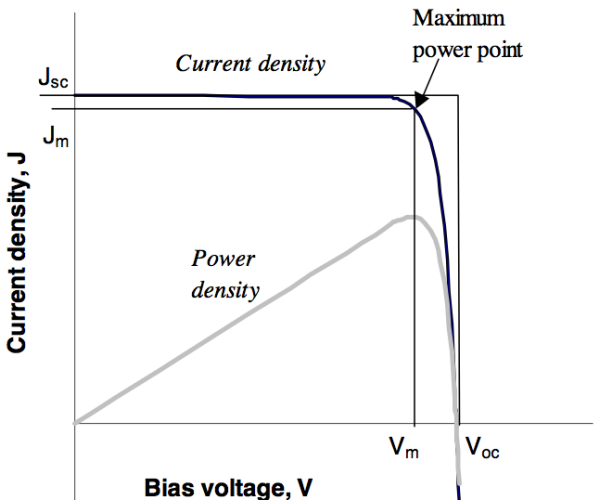

Figure 2.2: The current density and the power density plotted against the voltage of an ideal solar cell [10].

2.2 Luminescent Solar Concentrators (LSC)

A typical Luminescent Solar Concentrator consists of a polymer plate doped with luminescent material. Photons travelling towards the top surface of a polymer plate will be reflected or transmitted through the plate following the Fresnel equations. When transmitted the photon will change its direction with respect to the normal of the surface, following Snell's law:

$$\frac{\sin\theta_i}{\sin\theta_t} = \frac{n_2}{n_1} \tag{2.7}$$

θ_i is the angle of incidence, θ_t is the transmitted angle and n is the refractive index of the respective medium. When not absorbed the photon will, due to symmetry, travel through the plate, and exit through the bottom surface. The reflection coefficient can be calculated by the formulas 2.8 and 2.9 depending on the polarisation of the light. The light is s-polarised when its electric field is in the plane of the interface between the two media and p-polarised when its electric field is perpendicular to the interface plane.

$$R(s) = \left[\frac{n_1\cos\theta_i - n_2\cos\theta_t}{n_1\cos\theta_i + n_2\cos\theta_t}\right]^2 \tag{2.8}$$

$$R(p) = \left[\frac{n_1\cos\theta_t - n_2\cos\theta_i}{n_1\cos\theta_t + n_2\cos\theta_i}\right]^2 \tag{2.9}$$

For a practical use of LSCs it is safe to assume that the light is unpolarised, for which the average of the

two equations can be taken [5].

The LSC has a refractive index higher than air, typically around 1.5 for mostly used plastics such as PMMA, and therefore acts as a die-electric waveguider. According to the Fresnel equations, when light travels from a medium with a higher refractive index to a lower refractive index medium, a critical angle with respect to the normal exists for which every photon will be reflected. The critical angle (θ_c) is given by arcsin(1/n). This effect is depicted in figure 2.3.

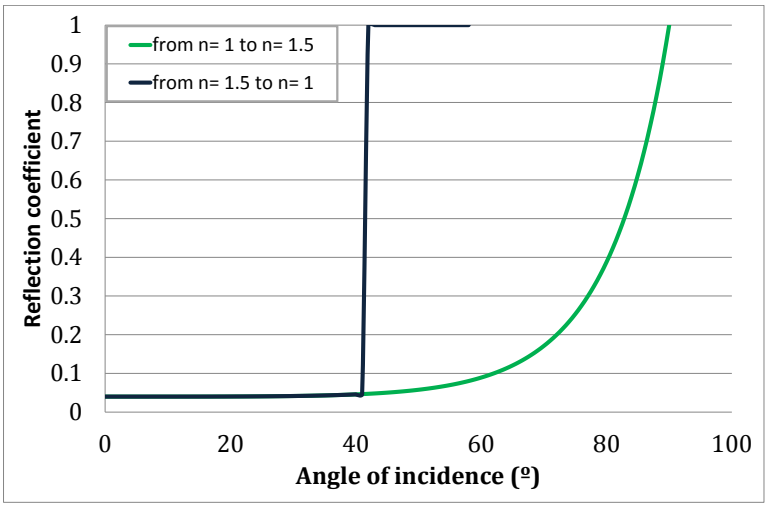

Figure 2.3: The reflection coefficient for photons travelling from a medium with a refractive index of 1 to a medium with refractive index of 1.5 and the reflection coefficient travelling in the opposite direction.

When a photon is absorbed and emitted isotropically by a luminescent centre, it can be trapped within the plate, when emitted with an angle larger than the critical angle. This effect is called total internal reflection (TIR). These photons will be wave guided to the edges of the plate. With light shining on the top surface of the plate, the geometrical gain (G) between the top surface and the edges leads to concentration of the light. In the case of a cylinder, with length l and radius r, the geometrical gain is given by equation 2.10.

$$G = \frac{A_{in}}{A_{out}} = \frac{2rl}{2\pi r^2} \tag{2.10}$$

The optical efficiency is defined as the amount of photons collected at the edge of the LSC devided by the total amount of photons incident on the LSC. Multiplying the optical efficiency with the geometric gain,

gives the optical concentration (C) of the device [5].

$$C = \eta_{\text{opt}} G \tag{2.11}$$

2.3 Luminescent Centres

Different types of material can absorb and emit light but not all are suitable to use for LSC applications. Research is performed on LSCs with quantum dots, rare earth materials, nanorods and semiconducting polymers as luminescent material but during this research the focus will be on organic dyes, specifically lumogen-red dye. In an organic dye, a photon can be absorbed by transferring its energy to an electron in the lowest unoccupied molecular orbital (LUMO), exciting it to the highest occupied molecular orbital (HOMO). This occurs when the photon has an energy equal or greater than the energy band gap between the HOMO and the LUMO. Vibrational and rotational degrees of freedom induce many sub energy levels around the LUMO and the HOMO.

Generally, the life time of excited electronic states is several nano-seconds. Vibrational interactions occur quicker than that, causing the excited electron to lose its excess energy, the difference between photon and band gap energy ($hv - E_g$), and to thermalise to the bottom of the HOMO level. When the HOMO state is weakly coupled to a non-radiative decay path, electrons can combine radiatively. The photon emitted will always have an energy lower than the photons absorbed. The energy difference between the absorption peak and the emission peak as a result, is called the Stokes shift. The excited electron can lose its energy via non-radiative processes as well. The ratio between the emitted photons and the absorbed photons determines the luminescent quantum efficiency (LQE).

There are four important requirements of LSC luminescent centres:

- A broad absorption spectrum and a narrow emission peak with a wavelength just below the band gap of the solar cell. When using a silicon solar cell, absorption up to λ=950 nm and an emission peak $\sim$1000 nm would be ideal.
- A large Stokes shift, which will reduce re-absorption of emitted photons
- High luminescent quantum efficiency
- Stable material, especially when exposed to the sun

Organic dyes have a near unity quantum yield in the UV-visible range, are stable for many years when using glass or PMMA as an host material and the overlap between the absorption and the emission spectra is small compared to quantum dots but large compared to conjugated polymers or rare earth materials[11]. Typically the absorption spectrum of an organic dye is not very broad (<100nm) but this issue could be

overcome when using multiple dyes with different absorption spectra[12].
The amount of photons that are absorbed depends on the absorption coefficient of the material and the path length according to the Beer-Lambert law:[11]

$$\frac{I_\lambda(x)}{I_\lambda(0)} = e^{-\alpha(\lambda)x} \tag{2.12}$$

Here α is the absorption coefficient, related to the density of luminescent centres and the wavelength of the incoming light, $I_\lambda(0)$ is the initial light intensity and $I_\lambda(x)$ is the attenuated light intensity after travelling through thickness x. The absorption coefficient and the path length are important characteristics of a LSC and varying these characteristics will change the optical efficiency severely.

2.4 Optical Efficiency

The optical efficiency, defined in paragraph 2.2 can be calculated by multiplying the capture efficiency with the wave guide efficiency

$$\eta_{\text{opt}} = \eta_{\text{capture}}\eta_{\text{waveguide}} \tag{2.13}$$

The capture efficiency exhibits the fraction of the photons that are absorbed by the luminescent centres. Photons that are not absorbed can either be reflected or transmitted through the LSC but in either way they will not be wave guided to the edges and thus not contribute to the total efficiency. The wave guide efficiency takes into account the losses that occur after absorption. The absorbed photons can be emitted with an angle smaller than the critical angle, which is referred to as the escape cone. They will not be subject to TIR and therefore lost. For a flat plate the photons that are trapped by after emission are defined by the critical angle as follows [13]:

$$\eta_{\text{trap}} = 1 - \eta_{\text{escapeconeloss}} = 1 - \frac{4\pi \int_0^{\theta_c} d\theta \sin\theta}{4\pi} = 1 - (1 - \cos\theta_c) = \sqrt{1 - \frac{1}{n^2}} \tag{2.14}$$

A glass or PMMA plate, which has a refractive index of 1.5 has an trapping efficiency (η_{trap}) of 74% . When the dye has a non-unity quantum efficiency (η_{QY}) not all photons are emitted, resulting in a lower wave guide efficiency. Emitted photons can be re-absorbed ($\eta_{reabs} = 1 - \eta_{nonreabs}$) again by the dye when emitted with an energy larger than the energy difference between the HOMO and the LUMO level. These photons will again face the chance to be emitted within the escape cone or not be emitted at all. The last loss that should be taken in to account is absorption by the host material. PMMA or glass can absorb light too but they are unable to emit light and thus these photons are lost ($\eta_{nonabshost}$). Overall the efficiency is given by:

$$\eta_{\text{opt}} = \eta_{\text{capture}}(\eta_{\text{QY}}\eta_{\text{trap}}\eta_{\text{nonreabs}}\eta_{\text{nonabshost}} + (1 - \eta_{\text{nonreabs}})\eta_{\text{QY}}\eta_{\text{trap}}\eta_{\text{nonreabs}}\eta_{\text{nonabshost}}...) \tag{2.15}$$

Depending on how often a photon can be reabsorbed, which depends on the Stokes shift, this equation will have to be extended. In figure 2.4 all the different processes described are depicted for a fibre LSC. In the next chapter a more detailed description of how these processes work specifically for an LSC with a fibre geometry will described and the losses will be quantified where possible.

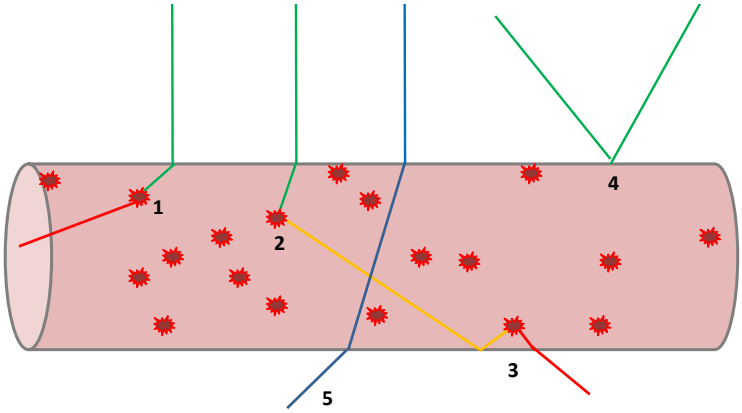

Figure 2.4: Photon interactions in a fibre LSC: 1) photon is absorbed and emitted with a lower energy in the direction of the edge, 2) photon is absorbed and emitted with an angle causing TIR, 3) this photon is re-absorbed again but now emitted within the escape cone, 4) photon is reflected, 5) photon is not absorbed and thus passes through the LSC without being wave guided.

2.5 State of the Art

The concept of a luminescent solar concentrator was first published in the late 1970s and was intensely studied in the first years after that point but due to limitations of the luminescent material it seemed impossible to achieve high enough efficiencies and research stagnated. In the last decade there has been a renewed interest in LSCs as new options for luminescent materials have arisen and different designs are being tested[11]. In this paragraph a few of the newest developments are discussed.
Research has been performed on LSCs where the luminescent material is deposited on a thicker transparent plate. As the absorption and emission is confined to the thin film this configuration is proposed to reduce the re-absorption losses. To achieve the same amount of absorption, the concentration of the luminescent material must be higher in the thin film than it was in the classical LSC, inducing higher re-absorption losses in the thin film layer itself. Research has shown that this configuration does not necessarily increase the optical efficiency of the LSC [5].
In a high dye concentrated layer on the other hand, the possibility exists that cascaded emission occurs via non radiative Förster resonant energy transfer (FRET). Currie et al. reported a 6.8% projected power conversion efficiency for a LSC system, where FRET took place, containing two thin film plate LSCs placed on top of each other, with an air gap between them [14].The set-up is depicted in figure 2.5.

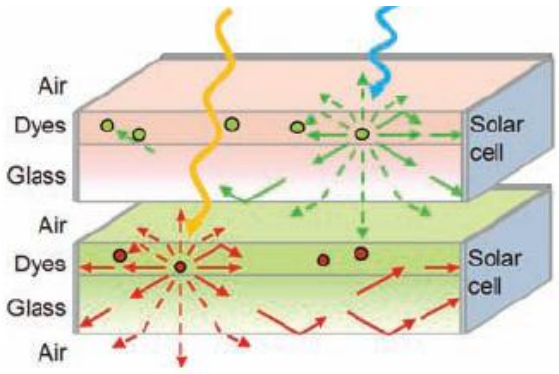

Figure 2.5: Two thin film LSCs containing organic dyes on high refractive index glass substrates as proposed by Currie et al.[14].

To increase the absorption range of the LSC multiple dye systems have been proposed. Several layers with dyes with a different absorption range enhances the chance that a photon is absorbed. Short wavelength photons can be absorbed by different molecules than long wave photons. Short wave length photons will most likely be absorbed several times by increasingly longer wave length dyes before they reach the edge of

the LSC in this configuration [11].

An approach to decrease the escape cone losses is found by using frequency selective mirrors and placing them on the surface where the light enters the fibre. Photons departing the LSC through the escape cone will have a longer wavelength than the incident photons that can be absorbed. The mirror selectively reflects the longer wavelengths back to the LSC while short wavelength incident light is transmitted through the mirror [11].

In this research the aim is to investigate if the concentration ability of the LSC can be increased by changing the geometry from a plate to a cylinder as proposed by McIntosh [4]. Hereby specifically it will be researched if by increasing the length and decreasing the radius, ultimately attaining the dimension of a fibre, the configuration becomes more efficient.

Chapter 3

Theoretical Comparison

In this chapter the classical flat plate geometry will be compared with the cylindrical geometry. The path of the photon incident on a cylindrical and a flat plate LSC will be analysed theoretically to get a better understanding of the working mechanisms and the differences between the two. The analysis will be done following the calculations of McIntosh [4] and extending them where possible.

3.1 Comparing Losses

Changing the LSC shape will change the optical efficiency as the losses caused by reflection, host material absorption and the escape cone losses are different. The quantum yield dependence on the LSC shape is negligible and will not be taken in to account during this comparison. Re-absorption losses depend on the path length after being absorbed and therefore the geometry of the LSC. However during this calculation it is assumed that the concentration of luminsecent species is low and this loss is not taken in to account. It is assumed that the host material has a refractive index of 1.5, incident rays have an equal amount of transverse electric (TE) and transverse magnetic (TM) polarisation and the volume of the cylindrical and plate LSC is the same.

3.1.1 Reflection

As explained in Chapter 2 the reflection of a medium can be calculated by the Fresnel Equations and is dependent on the refractive index of the medium and the angle of incidence. Only the direct light will be analysed in this paragraph as the diffuse light will be incident from every angle. For direct light on the plate LSC the angle of incidence is the same on every point of the surface. For the cylindrical LSC this is not the case as the normal vector varies over the surface of the LSC. McIntosh calculated the reflection for the cylindrical and plate LSC, assuming radiation at normal incidence, originating from a planar source. In

this case the reflection was 4% for a flat plate and averaged over the cylinder surface it was 6.9% [4].
In reality the suns position is not perpendicular to the surface the whole day, when there is no tracking mechanism used. The position of the Sun with respect to the surface of the earth can be described by the solar zenith angle (θ_z) and the solar azimuth angle (A) as can be seen in figure 3.1 [6].

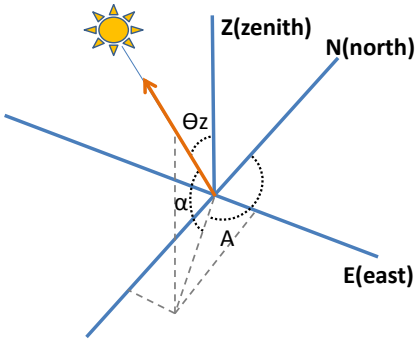

Figure 3.1: Coordinate system for an observer standing in the origin, with θ_z is the solar zenith angle and A the solar azimuth angle. α, the solar altitude angle is π-θ_z.

The solar vector S pointing towards the earth can be described by:

$$S = \begin{pmatrix} \sin(\alpha) \\ \cos(\alpha)\sin(A) \\ \cos(\alpha)\cos(A) \end{pmatrix}$$

in this z, e, n coordinate system. The solar zenith angle and the solar azimuth angle are calculated for the 21st of June and the 22nd of December at every hour in London [7]. For a horizontal plate at the origin, the cosine of the angle between the central ray of the Sun and the flat plate angle can be expressed as: $\cos(\theta_i) = \sin(\alpha)$. The plate can also be placed with a tilt angle (β) and a plate azimuth angle (γ). The incident angle for a vertical plate facing the south can be described by equation 3.1 and for a general tilted plate by 3.2.

$$\cos\theta_i = \cos\alpha\cos(\gamma - A) \tag{3.1}$$

$$\cos\theta_i = \sin\alpha\cos\beta - \cos\alpha\sin\beta\cos A \tag{3.2}$$

Using these equations the direct light reflection losses of a flat plate on a summer and a winter day can be calculated for different orientations. In this study a horizontal, vertical and 52 degrees tilted plate in London, weighted for the photonflux per hour, have been compared. The reflection coefficient per hour can be found in Appendix A. The results attained are shown in the following table.

Reflection coefficient			
	21 Dec		21 June
horizontal plate	32.2 %	horizontal plate	7.0 %
vertical plate	4.1 %	vertical plate	36.8 %
tilted, 52 degrees	4.3 %	tilted, 52 degrees	14.6 %

Table 3.1: The reflection coefficient of a flat plate LSC on the 22nd of December and 21st of June.

It can be seen from these results that taking the position of the flat plate and the time of year into account is very important as is makes a large difference to the reflection losses. The horizontal plate has the least amount of reflection losses in the summer because the Sun is incident on it the whole day while the tilted and the vertical plates will have the Sun pointing at their back in the beginning and at the end of the day. Overall, averaging the losses weighted by the photonflux, the horizontal plate is the most efficient, with an average reflection coefficient of 9,45 %.

For the cylindrical LSC the reflection calculation is less obvious. When the cylindrical LSC is aligned with the North-South axis the Sun will turn around it in during the day, always pointing towards it. The cosine of the angle between the central ray of the Sun and the North-South axis = $\cos\alpha \cos A$. A new coordinate system can now be analysed with the suns vector lying in the xz plane and the LSC normal lying in the yz plane following figure 3.2.

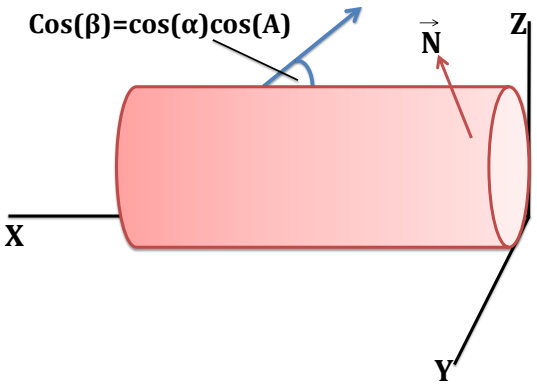

Figure 3.2: The vector pointing towards the Sun, having an angle $\cos(\beta)$ with the x-axis and the surface normal vector in the y-z plane.

The angle between these two vectors varying the distance y on the LSC and varying the time of the day,

Reflection coefficient			
	21 Dec		21 June
aligned North-South	17.6 %	aligned North-South	14.6 %
aligned East-West	16.2 %	aligned East-West	16.1 %
tilted, 52 degrees	14.5 %	tilted, 52 degrees	15.2 %

Table 3.2: The reflection coefficient of a cylinder LSC on the 22nd of December and the 21st of June.

can be calculated for the cylindrical LSC reflection coefficient for the same two days. In a similar way the reflection coefficient for a fibre lying aligned with the east-west axis and fibre tilted 52 degrees facing the south has been calculated and the results can be found in table 3.2

It can be seen that the reflection coefficient of the fibre is more stable throughout the year as well as when placed at different positions than the plate LSC. The average reflection coefficient for these two days is the least for the fibre aligned North South, with a value of 14,9%. With these results it can be concluded that the flat plate has a lower reflection coefficient when placed on a horizontal surface than the fibre but that the reflection coefficient of the fibre fluctuates less.

3.1.2 Total Internal Reflection

In paragraph 2.4 the trapping efficiency for a flat plate has been calculated. The critical angle is the same for the cylindrical LSC but the proportion of the light emitted reaching the surface with an angle larger than the critical angle is different. In a flat plate this does not depend on where the luminescent centre is located within the plate, it depends solely on the refractive index of the host material. According to equation 2.14 for a refractive index of 1.5 the trapping efficiency is 74%.

In a cylindrical LSC the trapping efficiency does depend on the position of the luminescent centre. It is easy to picture that a luminescent centre located close to the surface will have an escape cone similar to the flat plate, while when located in the centre, all the emitted photons in the yz plane will escape. Considering a infinitely long cylinder, the escape cone of a luminescent centre can be defined dependent on the distance r to the centre. The trapping efficiency calculation was carried out in collaboration with Luca Patrignani, a student working on his Optics and Photonics MSc project in Dr Chatten's group.

A cylinder is placed in a x, y, z coordinate system with the cylinder axis placed parallel to the z axis, going from $-L$ to $+L$. The origin is fixed at the location of the luminescent centre. The photon emitted by the luminescent centre will hit a generic point on the surface called $P(x, y, z)$. The normal at this point P has the direction $(x, y + r, 0)$. To find for which points the scalar product between the vector going from the

origin to P and the normal vector is greater than the critical angle, a system has to be solved with the following requirements:

$$\begin{cases} x^2 + (y+r)^2 = R^2 \\ -L \leq z \leq L \\ \frac{x^2+y^2+yr}{\sqrt{x^2+y^2+z^2}\sqrt{x^2+(y+r)^2}} = \sqrt{1-\frac{1}{n^2}} \end{cases} \tag{3.3}$$

where the first two originate from fixing point P on the surface of the cylinder and the third from the scalar product of the two vectors. The solution is the following, of which the derivation can be found in the Appendix B:

$$\Rightarrow \begin{cases} y = \frac{R}{\rho}\left[\frac{1}{n^2} - \rho^2 \pm \sqrt{\left(1-\frac{1}{n^2}\right)\left(\rho^2 - \frac{1}{n^2} + \frac{z^2}{R^2}\right)}\right] \\ x = \pm\frac{R}{n\rho}\sqrt{\rho^2 + 1 - \frac{2}{n^2} - \frac{z^2}{R^2}(n^2-1) \mp 2\sqrt{\left(1-\frac{1}{n^2}\right)\left(\rho^2 - \frac{1}{n^2} + \frac{z^2}{R^2}\right)}} \\ -L \leq z \leq L \end{cases} \tag{3.4}$$

with $\rho = r/R$, the radius,$\in [0;1]$. Solutions for x and y exist for

$$z^2 \geq R^2\left(\frac{1}{n^2} - \rho^2\right) \tag{3.5}$$

so for $\rho > 1/n$, solutions are found $\forall z$. This condition is translated to spherical coordinates in order to integrate over different angles, which gives the following result:

$$\Rightarrow \cos\phi = \sqrt{1 + \frac{1}{n^2\rho^2}\left(\frac{n^2-1}{\tan^2\theta} - 1\right)} \tag{3.6}$$

Assuming a isotropic emission, the trapping efficiency can now be calculated by integrating as

$$\eta_{\text{trap}} = \frac{1}{4\pi}\iint \sin\theta d\theta d\phi \tag{3.7}$$

For every emission point in the cylinder a photon can escape directly to the edges through two double cones, which are symmetric with respect to the emission point. Therefore θ can be restricted by [0; $\pi/2$] for the integration, when a factor of 2 is included.

In the chosen coordinate system, the cone pointing towards the positive z is spanned by θ going from 0 to $\pi/2 - \theta_c$, where θ_c is the critical angle. Over this range, the integration over ϕ will always give 2π, regardless of the position of the emission. This gives a constant result, which induces a lower limit to the trapping efficiency:

$$\eta_{\text{trap}}^{\text{const}} = 2 \times \frac{1}{4\pi} \int_0^{\pi/2-\theta_c} 2\pi \sin\theta d\theta$$

$$\Rightarrow \quad \eta_{\text{trap}}^{\text{const}} = (-\cos\theta)\Big|_0^{\pi/2-\theta_c} \quad \Rightarrow \quad \eta_{\text{trap}}^{\text{const}} = 1 - \sin\theta_c$$

$$\Rightarrow \quad \eta_{\text{trap}}^{\text{const}} = 1 - \frac{1}{n} \tag{3.8}$$

For n= 1.5 the lower limit is 33.89%, which is the minimum trapping efficiency, in other words the trapping efficiency for a point on axis. When the emission point is located further away from the axis, there will be other regions for θ and ϕ for which the emitted photon will be trapped as well. These regions will lie in the range of $\theta \in [\pi/2 - \theta_c; \pi/2]$, the region that has not been accounted for by $\eta_{\text{trap}}^{\text{const}}$.
For this part of the integration equation 3.6 has to be taken in to account, depending on ρ. When plotting the angular solution of ϕ it is found that ϕ is also symmetrical with respect to $\pi/2$. Therefore the integration can once again be simplified. The integral has to be split in to section depending on ρ. For $\rho < 1/n$ no solutions can be found in the circular cross section while for $\rho > 1/n$, θ can be integrated up to $\pi/2$. The upper limit for θ in the case that $\rho < 1/n$ can be found by solving Eq. 3.6 for $\phi = \pi/2$. This following solution is found:

$$\theta_{\max} = \arctan\sqrt{\frac{n^2-1}{1-n^2\rho^2}} \tag{3.9}$$

Now the integral is finalised and integration over ϕ up to $\pi/2$ multiplying the result by a factor of 4 yields:

$$\eta_{\text{trap}} = \eta_{\text{trap}}^{\text{const}} + \frac{8}{4\pi} \begin{cases} \int_{\pi/2-\theta_c}^{\theta_{\max}} \sin\theta \left[\frac{\pi}{2} - \arccos\sqrt{1 + \frac{1}{n^2\rho^2}\left(\frac{n^2-1}{\tan^2\theta} - 1\right)}\right] d\theta, & \text{for } \rho < \frac{1}{n} \\ \int_{\pi/2-\theta_c}^{\pi/2} \sin\theta \left[\frac{\pi}{2} - \arccos\sqrt{1 + \frac{1}{n^2\rho^2}\left(\frac{n^2-1}{\tan^2\theta} - 1\right)}\right] d\theta, & \text{for } \rho \geq \frac{1}{n} \end{cases} \tag{3.10}$$

This is the solution for η_{trap} as a function of just n and ρ. It can be used for any emission point in the fibre except when very close to the edge of the fibre. In that case the trapping efficiency would in fact be higher. The solution for three emission points lying in the three different integration regions is visualised in figure 3.3

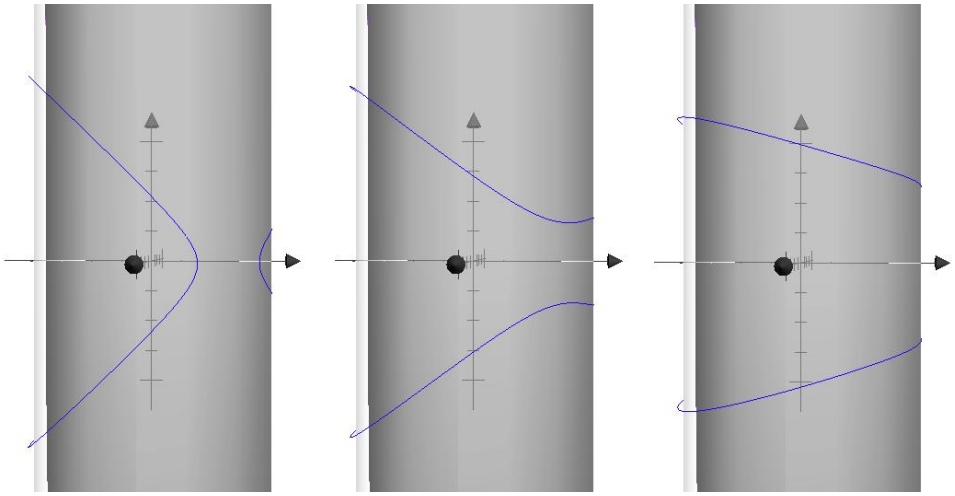

Figure 3.3: Escape region in a cylinder. From left to right the emission point is at a normalised distance of 0.7, 0.6 and 0.3 from the centre in the direction of the horizontal arrow, with n = 1.5. The blue line distinguishes between the region where the emission is trapped and where the emission escapes. In the left picture trapping occurs within the cylindrical interface and an escape cone similar to the escape cone in a flat plate exists with respect to the surface on the right side. In the right picture trapped emission only occurs in the direction of the edges.

In this report we took a different approach to the system than McIntosh, which we find more insightful, but the values attained are exactly the same. The results for the trapping efficiency with respect to the normalised distance to centre of the cylinder are depicted in figure 3.4. As is visible in the figure the closer the luminescent centre is to the surface, the higher the trapping efficiency is. Placing the luminescent centres at the surface of the cylinder would result in the highest trapping efficiencies. For this reason it would be interesting to compare homogeneous doped fibres with coated fibres.

The average $\bar{\eta}_{\text{trap}}$ for the fibre, assuming uniform density of the emission points is calculated as well. In this case the integration has to be carried out over $\mathrm{d}\rho^2$ instead of $\mathrm{d}\rho$, result are shown in figure 3.5. As expected the thinner the coating, the higher the trapping efficiency. At the same time it is visible that in a homogeneously doped fibre the trapping efficiency is 60%.

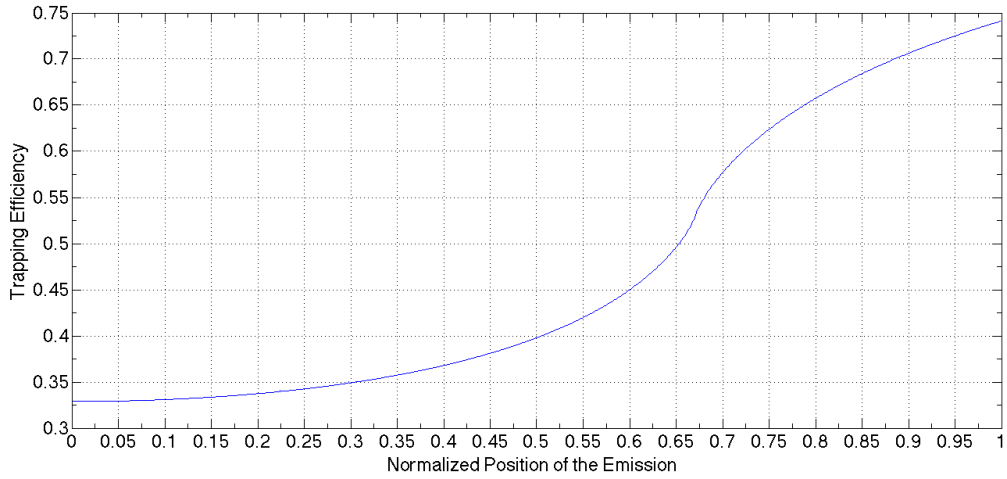

Figure 3.4: Trapping efficiency in an infinite long cylinder depening on the distance to the center.

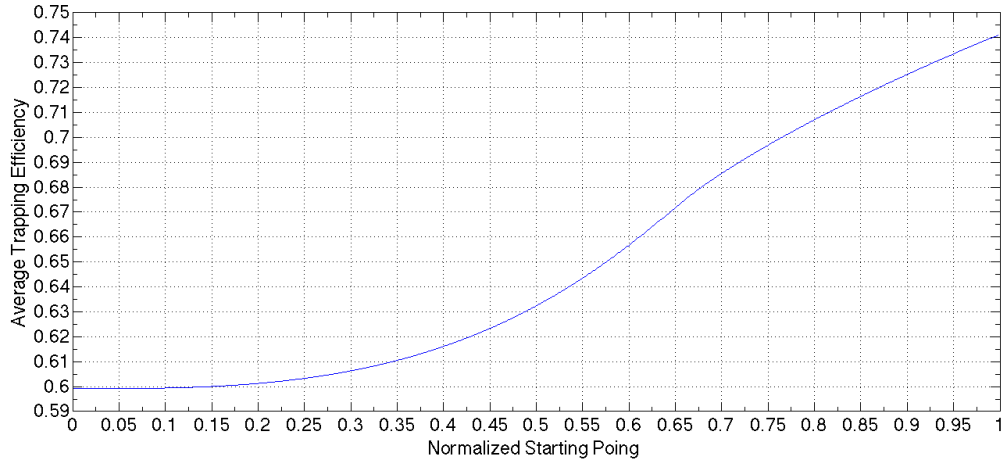

Figure 3.5: Average trapping efficiency while varying the radius up to which the coating extents. The point where the coating starts, with respect to the centre of the cylinder, is shown on the x-axis, ultimately ending with a homogeneously doped fibre at normalised starting point of 0.

3.1.3 Host Material Absorption

The host absorption depends on the emission angle, the absorption coefficient of the host material, the location of emission and the distance that the photon travels through the LSC. Assuming the emission

is isotropic and that the edges do not reflect the light back into the fibre, McIntosh calculated the host absorption for the absorption coefficient times the LSC length. For the cylindrical LSC they analysed this for the situation where r = 0 and r = R. McIntosh measured the absorption coefficient of PMMA to be 0.1 m^{-1} at 550 nm. When using this value a fibre with a length between 10-50 cm the host absorption will be between 1.1 and 7.8% for r = R, between 0.4 and 2.7 % for r = 0 and for a plate between 0.3 and 2.5%. The host absorption is higher at r = R because the fraction of oblique rays is higher than at r = 0. Oblique rays, undergoing TIR travel with a long helical path and therefore have a longer path length and thus a higher chance to be absorbed by the host material. In comparison if the PMMA has an absorption coefficient of 1 m^{-1}, for a fibre of 10-50 cm the host absorption will be between 14 and 38 % for r = R, between 4 and 20 % for r = 0 and for a plate between 5 and 23%

3.1.4 Overall Comparison

The main advantage of a fibre LSC over a plate LSC is that it has a higher geometrical concentration ratio, in other words the ratio between the module area, where light is incident, and the cell area is higher. For a cylinder this is defined by:

$$G_{cyl} = \frac{2RL}{2\pi R^2} = \frac{L}{\pi R} \tag{3.11}$$

For the plate LSC, assuming the plate is square, it is defined by:

$$G_{square} = \frac{L^2}{4LW} = \frac{L}{4W} \tag{3.12}$$

To compare the two shapes the volumes have to be identical, as the volume has a large contribution to the LSC costs. In addition the LSCs must have the same collection area. Combining these two assumptions gives the relation:

$$W = \pi R/2. \tag{3.13}$$

Inserting this condition into formula 3.11 gives

$$G_{cyl} = \frac{L}{2W} = 2G_{square} \tag{3.14}$$

which implies that the cylindrical geometrical concentration ratio is twice as large as the square one.
Combining all the results attained in this paragraph for the reflection loss, escape cone, host absorption and the geometric concentration the overall optical concentration ratio between the two shapes can be calculated. Taking the average reflection loss, the average escape cone loss for a homogeneous doped LSC and host absorption loss, assuming the absorption coefficient is 0.1 m^{-1}, the fibre is calculated to have an optical concentration which is 1.5 times as high as the optical concentration of the plate LSC. This is the case for an emission point at r = R and an emission point at r = 0. Even though the reflection loss, the

host absorption loss and the escape cone loss are larger in the fibre, due to a twice as large geometrical concentration, the overall optical concentration in a fibre is higher than in the plate LSC. For a higher host absorption the fibre is still more efficient. A host absorption coefficient of 1 m^{-1} for emission point at r = 0 results in 1.5 times as higher optical concentration of the fibre LSC as well. However when the emission point is then at r = R, the difference in host absorption between the two geometries is larger, resulting in a 1.3 times as efficient LSC fibre compared to the plate. This calculation assumes either low doped LSC or large Stokes shift of the luminescent centres, where re-absorption, which is related to the geometry of the LSC, will not play a significant role.

3.2 Photon Path

The photon changes its direction when entering the fibre following the Snell's equation. The larger the distance on the y-axis, the larger the angle change, resulting in a focussing of the rays at the back of the fibre, as is depicted in figure 3.6.

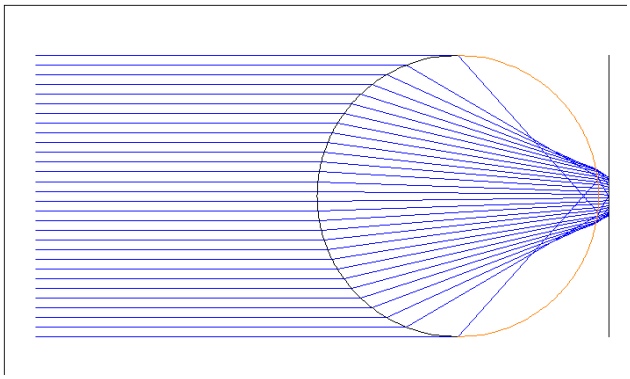

Figure 3.6: Path direction through the fibre, modelled by Zemax optical design [15].

It can be seen that the path length of the photons does not vary severely when changing the point where the photons hits the surface. The average path length is calculated to be 1,63 times the radius as can be seen in the appendix C. The path length affects the amount of photons absorbed according to the Beer-Lambert law equation 2.12 and should be taken in to account during the absorption calculations. Besides expecting that the coated fibre will be more efficient than the homogeneous fibre, it can also be expected that when only coating the backside partially of the fibre as depicted in figure 3.7, this configuration will be more efficient for the same amount of photons absorbed. In this case re-absorption losses are expected to be less, as the photons travel more through material not containing dye material and therefore the re-absorption losses are expected to decrease.

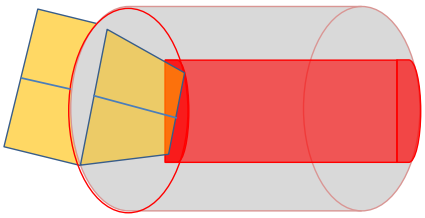

Figure 3.7: Light from a planar source is focused on the backside of the fibre, where only the red part is coated.

It is not possible though to focus the light in one point on the back of the cylinder by modifying the refractive index of the material because spherical aberration will always be introduced by the cylinder. Even so, by using a transparent polymer with a higher refractive index, the rays be bend more, resulting in a smaller focussing spot [15]. Often glass with a high refractive index, called flint glass, are harmful for human beings because they contain lead. In figure 3.8 an example of the focussing of a cylinder made of flint glass which is not harmful is depicted.

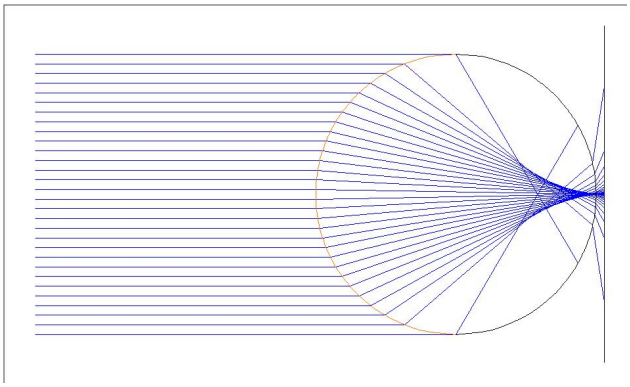

Figure 3.8: Path direction through the fibre made of flint glass with a refractive index of 1.95, modelled by Zemax optical design [15].

The calculation done in this section are specifically for normal incidence. Diffuse light shining on the fibre will not be focussed on the backside but will bend in different directions depending on the angle on incidence. To calculate the path length of diffuse light photons and for direct light photons which do not have a direction perpendicular to the cylinders axis, the third dimension will have to be taken in to account as well. This is outside the scope of this project but would be interesting to research in the future.

3.3 Summary

The reflection coefficient for a flat plate and a fibre on the 22nd of December and on the 21st of June have been calculated throughout the day in different positions. Placing the flat plate horizontal results in the lowest reflection losses with an average reflection coefficient of 9,45 %. Aligning the fibre with the North South axis minimizes the reflection losses and results in an average reflection loss of 14,9%. It is notable that the reflection coefficient of the fibre fluctuates less throughout the year when changing the position.
The trapping efficiency of the fibre has been found to vary with the distance r of the emission point to the centre of the fibre. The closer the emission point is to the surface, the higher is the trapping efficiency. Therefore it is expected that a PMMA fibre coated with lumogen red dye will be more efficient than a PMMA fibre with lumogen red dye spread homogeneously over the fibre. This will be tested during simulations the next chapter. The average trapping efficiency of a fibre with a refractive index of 1.5 is 60% while for the plate LSC it is 74%.
The host absorption in a fibre and in a plate have been compared following the method described by McIntosh (2007). Comparing the geometrical concentration of a fibre and a plate with identical volume and the same collecting surface area, the fibre has calculated to be twice as efficient as the plate. Combining this result with the trapping efficiency, reflection and host absorption losses, it is found that the fibre has an optical concentration which is 1.5 times as high as the plates optical concentration ability when the absorption coefficient of PMMA is assumed to be 0.1 m^{-1}. Note that homogeneous and low doping is assumed during this calculation, therefore re-absoption losses are not taken in to account.
Finally the average path length of a photon, with normal incidence, going through a fibre, without being absorbed, is calculated to 1.63 times the radius of the fibre. This result is important when determining the percentage of photons absorbed.

Chapter 4

Modelling of LSC fibres

The raytracing software PVtrace is used to simulate the behaviour of photons when travelling through the fibre LSC. This model is developed in python programming language by Daniel Farrell [16] and validated for flat plate LCSs [17]. It traces individual photon paths through the LSC and uses Monte Carlo methods to assign the outcome of events that the photon may experience. A few examples of such events are; whether a photon is absorbed and where it is absorbed, whether the photon is emitted and with which direction and wavelength. The input to the programme consists of absorption and emission data of the luminescent material, the direction and spectrum of the photon source, the absorption coefficient of the host material and the shape of the LSC. After having encountered an event a photon is labelled and when the simulation is finished, the amount of photons with a certain label can be counted, for instance the amount of absorbed photons going out of the left edge of the fibre.
For a few basic fibre LSC geometries the optical efficiency is first experimentally tested. These results will be compared to the same configurations, modelled by PVtrace. If the results are in agreement more complex structures, as for example the coated fibre, will be modelled and characterised. The results will hopefully give a better understanding of the working mechanisms of a fibre LSC and at the same time can verify if the hypothesis developed in Chapter 3 are correct.

4.1 Experimental Research

To verify if the data attained by PVtrace are viable, a few experiments are performed with homogeneous doped PMMA fibres with lumogen red dye. The homogeneous fibres that are used vary in length and in diameter. Overall, four different types have been tested with radius varying between 0.25 mm and 1 mm and length between 5.6 cm and 20 cm and a refractive index of 1.6, fabricated by Industrial Fibers Optics (IFO), USA [18].

4.1.1 Experimental Method

Several experiments have been performed to quantify the optical efficiency of the fibres tested and to characterise them. Before performing the actual optical efficiency measurement, the emission spectrum of the fibre and the spectrum of the light illuminating the fibre must be known. To compare the experimentally found with the modelled optical efficiency, the absorption spectrum, the absorption coefficient and the quantum yield of the dye must be measured, as these data must be input in the model to make a fair comparison. In addition the emission spectrum coming out of the fibre edges is measured. In this paragraph a short description of the experimental methods used are given.

4.1.1.1 Absorption and Emission

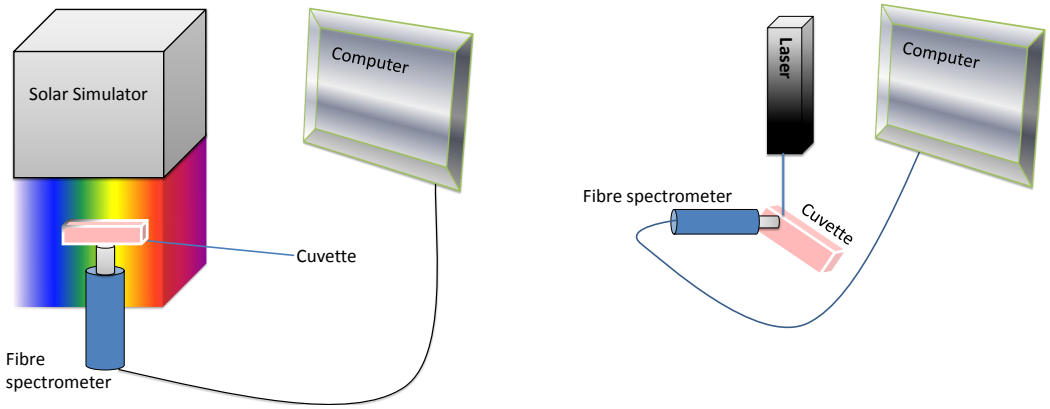

Figure 4.1: a, The set-up for absorption. b, The set-up for emission.

To measure the absorption and emission spectrum, and calculate the absorption coefficient, the fibre was first dissolved in chloroform. This mixture was put in a fused silica cuvette of high quality optical glass with low absorption in the UV-visible spectrum. For the absorption spectra the cuvette was placed under the class B solar simulator, manufactured by Steuernagel Lichtechnik (model:TCMG SOe MHL). A high resolution fibre spectrometer (Ocean Optics, HR4000CG-UV-NIR), with a wavelength range of 350 to 1000 nm, was used to measure the spectra of the light coming from the solar simulator and from the light going through the cuvette. Dividing the cuvette spectrum by the solar simulator spectrum provided us with the transmission per wavelength and with that the absorption coefficient per wavelength could be calculated, following the Beer Lambert Law, equation 2.12.

The emission per wavelength was calculated by using the laser as excitation beam, which pumped with a

wavelength of 473 nm. The laser pointed at the very edge of the cuvette while the same fibre spectrometer was used to collect the emission spectra on the other side of the edge. In this way the path length of the photons was minimised and with it the re-absorption chance. In figure 4.1 the two set-ups are depicted.

4.1.1.2 Optical Efficiency

The optical efficiency was measured by illuminating the fibre with the solar simulator, attaching a silicon solar cell against the edge of the fibre and measuring the short circuit current produced by the solar cell. To assure that there is no air gap between the solar cell and the edge of the fibre, refractive index matching fluid of the brand Cargille with a refractive index of 1.49 is used. The part of the solar cell which was not attached to the fibre was covered with black tape. Knowing the shape of the fibre emission spectrum, the quantum efficiency of the solar cell and the area of the edge of the fibre, the measured short circuit current can be converted to collected photons per second. To measure the amount of incoming photons the same approach was used, but now measuring the photons coming directly from the solar simulator. Dividing the total photons out by total photons in gives the optical efficiency.
In a similar way the laser has been used instead of the solar simulator as photon source. The distance between the point where the laser beam hits the fibre and the edge of the fibre has been varied to examine the role of host absorption and re-absorption by the dye.

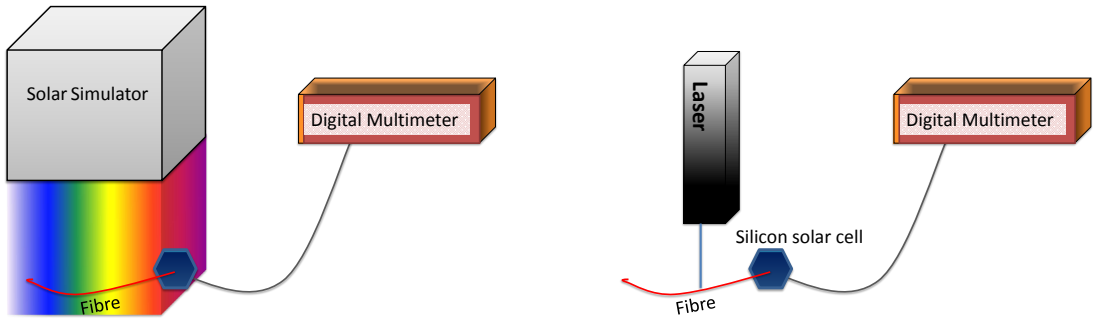

(a) (b)

Figure 4.2: Optical efficiency measurement with a, the solar simulator and b, the laser.

4.1.1.3 Luminescent Quantum Yield (LQY)

Several set-ups have been used to try to measure the quantum yield of the dye but no satisfying result was found. The first approach was to dissolve the fibre in chloroform and this mixture was brought into the Horibe UV vis 2000 spectrometer in a cuvette. Following the method described by Mello [19] three

measurements are performed: 1) laser beam directly hitting the sample in the integrating sphere, 2) sample placed in the integrating sphere but the laser beam is directed to the wall of the sphere, 3) measurement without the sample in the sphere. With these three measurements it should be possible to calculate the amount of photons absorbed and the amount of photons emitted by the sample and thus find the photo-luminescence quantum yield. The first approach with the cuvette did not work as it was impossible to place the cuvette in the integrating sphere in such a way that the laser beam hit it directly. In the second approach the mixture of fibre and chloroform was spin coated on a glass plate and placed in the integrating sphere of the UV vis. This time it was possible to perform the three measurements but the results were not satisfying. The quantum yield calculated had a value of 35% which is not in agreement with the literature values. Perylene dyes have a quantum yield between 90% and 100% [17]. It could be possible that the LQY changes when incorporating the dye into a polymer such as PMMA. It is known that excessive initiator can affect the quantum yield.[20]. On the other hand Wilson tested the LQY of lumogen red dye incorporated in a PMMA sheet and reported that the LQY was between 98 and 100% [21]. In this research it is assumed that the lumogen red dye has a quantum yield of 90%, which is the lowest literature value reported for a perylyne dye.

4.1.1.4 Emitted Spectrum

A set-up very similar to the optical efficiency set-up with the laser, is used to measure the emitted spectrum coming out of the fibre edge. Only here, instead of the silicon solar cell, the fibre spectrometer has been used to detect the photons coming out of the edge. The fibre spectrometer is placed facing the edge of the fibre, as close as possible to the edge. The position where the laser beam hits the fibre has been varied in this set up as well. The set-up is depicted in figure 4.3.

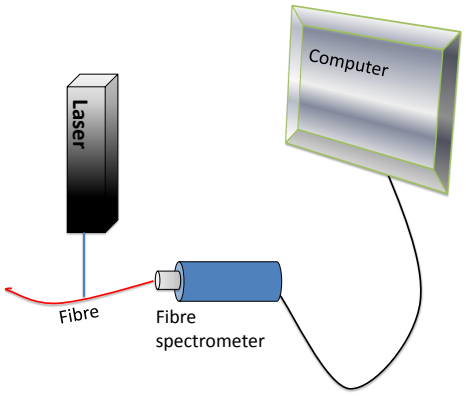

Figure 4.3: The set-up used to measure the emission spectrum.

4.1.2 Experimental Results

4.1.2.1 Absorption and Emission Spectrum

The results for the absorption and the emission spectrum data can be found in figure 4.4.

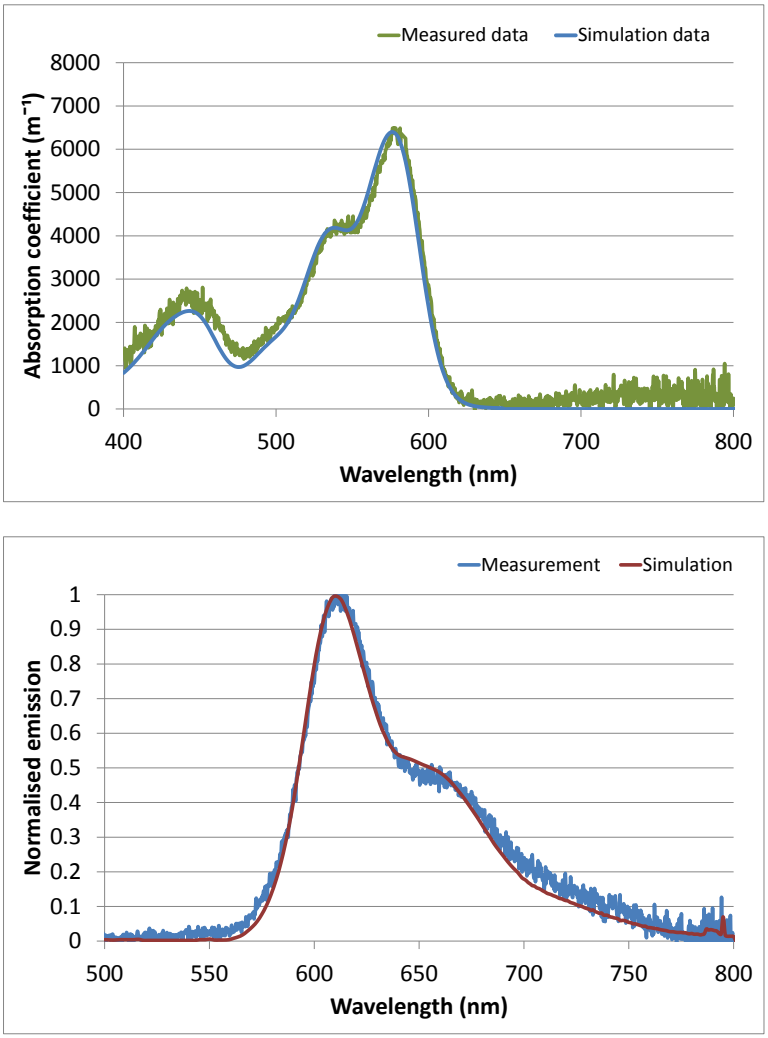

Figure 4.4: Top :Absorption spectrum of the fibre with a radius of 1 mm measured and used for the simulation with PVtrace. Bottom: Normalised emission spectrum of the fibre with a radius of 1 mm measured and used for the simulation with PVtrace. The peak at 473 nm are measured photons coming directly from the laser.

It can be seen that the absorption coefficient is 6400 m^{-1}.[1] In the figure the smoothed measured data is shown as well. This data is used during the simulations with PVtrace as absorption and emission spectrum of the modelled LSC.
The absorption coefficient for the 0.25 mm and 0.5 mm radius size fibre have been measured as well and turned out to be exactly the same. They can be seen in Appendix D. This is in line with our expectations as they are made from the same material. The measured data is in agreement with the literature absorption and emission spectra of lumogen red [17].

4.1.2.2 Optical Efficiency using the Solar Simulator

The optical efficiency of the fibres while illuminated by the solar simulator have been measured and compared to the optical efficiency results modelled with PVtrace. The results can be seen in the figure 4.5. For the simulation it is assumed that the host absorption coefficient is 1 m^{-1}, the absorption coefficient of the dye is 6400 m^{-1} and the quantum yield is 90%. The uncertainty of these assumptions are quantified in the error-bars. The photon flux spectrum produced by the solar simulator is measured with the fibre

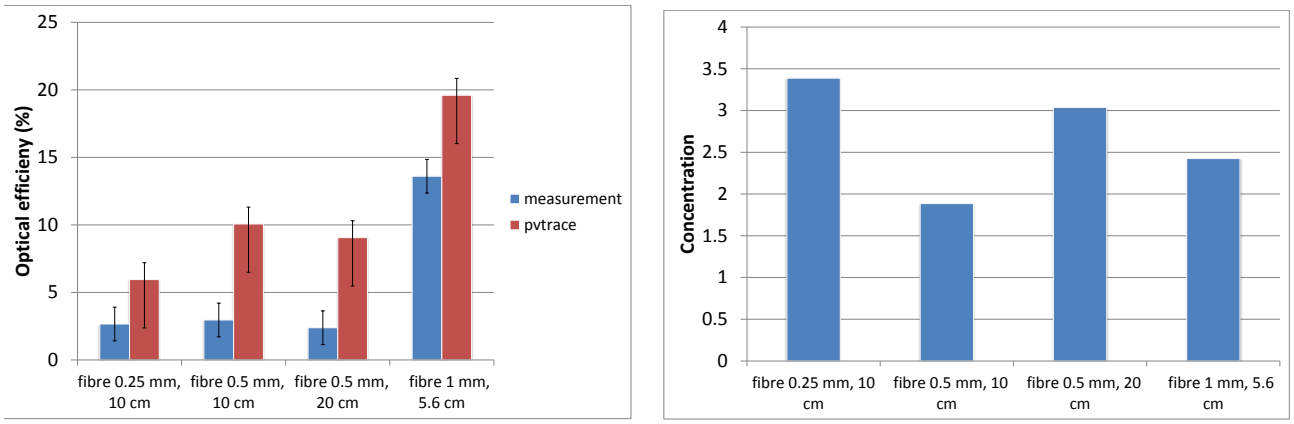

(a) (b)

Figure 4.5: In the left figure the optical efficiency for the four different LSC fibres, measured experimentally and simulated with PVtrace is depicted. In the right figure the concentration of the measured fibres can be seen.

spectrometer and is used as input for the source emission spectrum in the model. The solar simulator spectrum as measured can be found in the Appendix E.

[1] The absorption coefficient depends on the molar absorption coefficient and the concentration of the dye.

The data measured by the spectrometer has a large uncertainty for photons with a wavelength greater than 900 nm. Therefore it has been assumed that the photon-flux is zero after this point. The uncertainty of this assumption, taking the quantum efficiency of a silicon solar cell for wavelengths greater than 900 nm (~ 0.4) into account, is reflected by the large lower error-bar.
The figure shows that the modelled and experimental optical efficiency are not in very good agreement using the set up with the solar simulator. This could be due to the uncertainty in the solar simulator spectrum. Therefore the same experiment is repeated but with the laser as source, of which the wavelength of the emitted photons is well known, and the results can be seen in the next section. An other explanation could be that the LQY of the dye is lower than 90%, perhaps due to the incorporation in the PMMA.
It is interesting to see though, that the optical efficiency while changing the length of the fibre decreases less than the area ratio increases. This means that increasing the length of the fibre will increase the concentration.

4.1.2.3 Optical Efficiency using the Laser

The optical efficiency is measured while varying the distance from the incident laser beam to the edge of the fibre. The out coming photons are measured from that edge and divided by the incoming photons. The results are depicted in the figure 4.6. The fibre with 0.25 mm radius could not be used as the laser beam size was to large and not all photons hit the fibre.
The same assumptions as in paragraph 4.1.2.2 are made. The uncertainty in the experimental results was estimated by repeating the experiment several times. The possibility exists that even with the larger radius size fibres not all photons originating from the laser hit the fibre, which results in a larger top error bar. The results attained by the model and by experimental research are not in perfect agreement, but they do show the same trend and and the error bars do show overlap, especially for the 1 mm radius fibre case.The difference could be caused by the lower luminescent quantum yield of the dye, which should be investigated more thoroughly in the future.
The refractive index during the simulations has been assumed to be 1.5. In a later of this research stage of this research it was found out that the refractive index of the fibres produced by IFO [18] has an refractive index of 1.6. On the one hand this will result in a higher trapping efficiency, however it will also increase the reflection losses of incident light and it will induce a mismatch between the index matching fluid and the fibre edge resulting in reflection of photon exiting at the edges. For future research it would therefore be interesting to investigate how changing the refractive indec of the LSC fibre to 1.6 would impact the optical efficieny.
When increasing the distance betweer the laser beam the edge the optical efficiency decreases. When the photons have travelled a longer distance before being collected the chance that host absorption or re-absorption

takes place is higher. This decrease in optical efficiency appears to be smaller in the model. To get a better understanding of the absorption and re-absorption processes the emitted spectrum while varying the laser beam distance is investigated as well. Even so, overall the trend seem quite similar and therefore it can be concluded that the model represents working mechanisms of the fibre LSC well and that it can be used to simulate the fibre LSC.

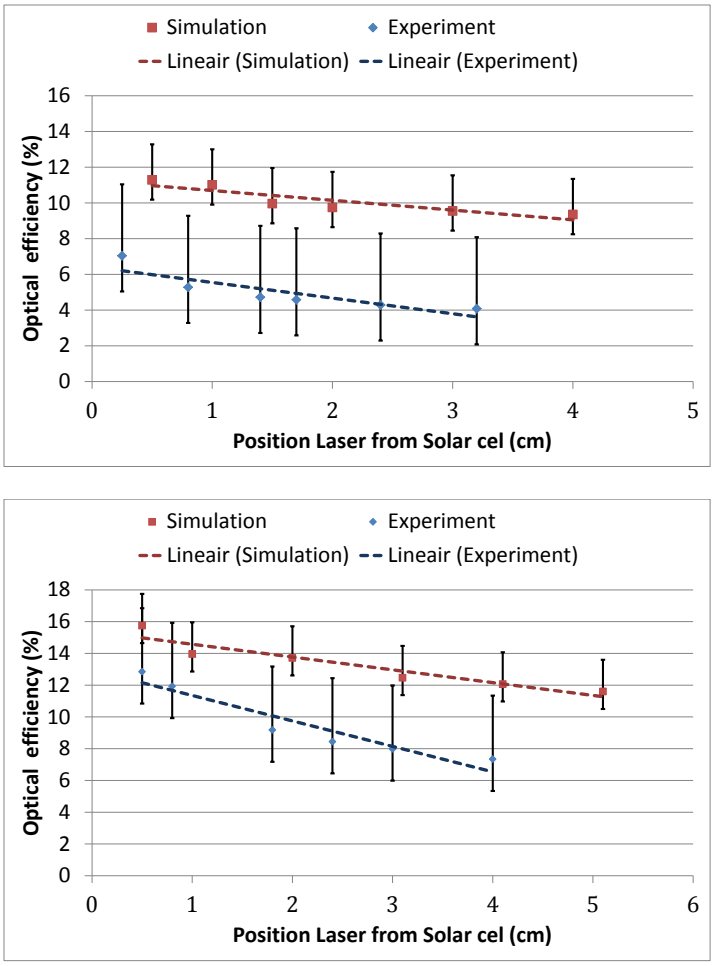

Figure 4.6: Optical efficiency, while varying the distance from the incoming laser beam to the edge, for a fibre with a radius of 0.5 mm (above) and 1 mm (below).

4.1.2.4 Emission Spectrum

In the figure below the modelled and the experimentally found emission spectra emitted from the edge of the fibre are shown. A clear red shift can be seen in both figures which is caused by the increasing

reabsorption when the distance between the laser beam and the edge is larger. The range of the spectrum is

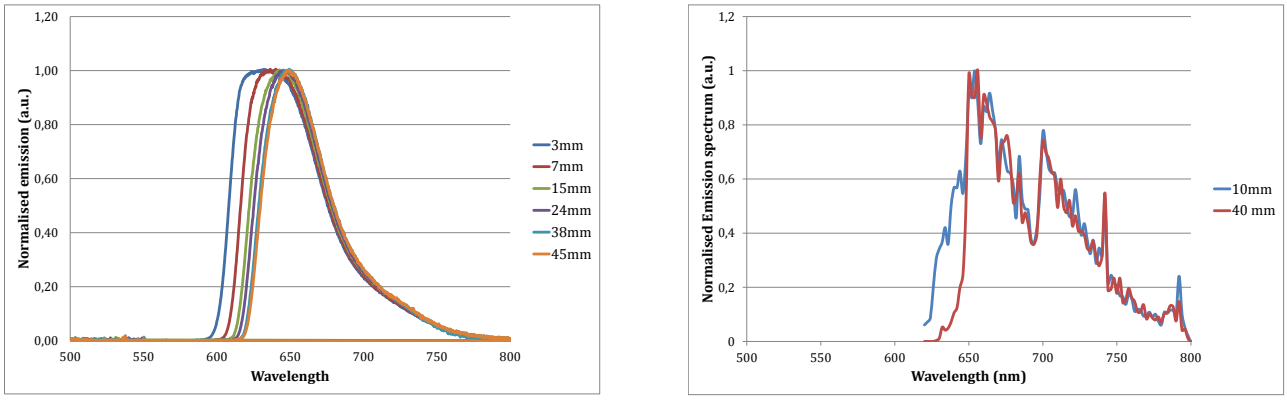

(a) (b)

Figure 4.7: Emissionspectrum exiting the edge of the fibre, with an absorption coefficient of 6400 m^{-1}, while varying the distance between the laserbeam and the edge. a, experimentally emeasured. b, modelled with PVtrace.

similar but the shape of the modelled emission spectrum is different from the experimentally found emission spectrum. For future research it could be interesting to investigate why this is the case and how this can be improved. Especially when the LSC has a very high optical density, the model is very sensitive for the emission and absorption data that are used as input. If, for example a small noise exist in the absorption data after 650nm, this can result in 100% absorption in this region, if the optical density is very high. In the data used the absorption spectrum was set to zero after this point. Therefore in this case this does not explain the discrepancy between the results, but it does illustrate that the model is sensitive at high optical density and that this sensitivity could perhaps be an explanation for the shape of the modelled emission spectrum.

4.1.3 Conclusion Experimental Verification

In this section the optical efficiency of four homogeneous doped LSC fibres have been calculated using PVtrace and by performing experimental research, after which the results have been compared. Using the solar simulator as source did not give a satisfying agreement and the uncertainty was quite large. This could be due to a high uncertainty of the photon flux produced by the solar simulator for wavelengths higher than 900 nm. For this reason a laser was used as a source while performing the same experiment. The results of the model were now in a better agreement with the experimental results and therefore the model can be

used to predict the concentrating potential of other LSC fibre configurations. The difference between the modelled and simulated results can be caused by a luminescent quantum yield lower than 90% of the dye. For future research it would be interesting to measure the LQY of the lumogen red dye in the PMMA fibre, as the incorporation of the dye into the polymer could possibly affect its LQY.

4.2 Simulations

Following the path of the photons through the fibre, characteristics such as optical efficiency, the concentration potential and percentage absorbed and re-absorbed are determined. First a homogeneously doped fibre is modelled and the effect of varying the optical density is analysed. These results are compared to the optical efficiency of a coated fibre, of which according to Chapter 3 it is expected that the coated fibre is more efficient. The length and the radius are varied to get a better understanding of absorption and re-absorption processes. In addition a half coated fibre mirror and a fibre partially coated, similar to the one depicted in figure 3.7 is simulated. Here the effect of placing a mirror behind the fibre will also be analysed. Finally, the optical efficiency increase of multiple fibres aligned will be modelled.
It is assumed that the host absorption is 0.3 m^{-1} and the quantum yield of the dye is 1. The AM1.5 spectrum is used as source spectrum up to 1100 nm. When using a silicon solar cell photons with a wavelength higher than 1100 nm will not have enough energy to excite the electron and therefore will not contribute to the electricity production. Even so, it must be taken into account that the optical efficiency values mentioned are optical efficiencies up to 1100 nm and that when taking the whole spectrum into account the optical efficiency will be lower.

4.2.1 Homogeneous Fibre and Coated Fibre

The coated fibre is expected to concentrate more efficiently per absorbed photon than the homogeneous fibre. In a coated fibre the emitted photons are always close to the surface and therefore have a smaller chance to escape, according to the calculations made in paragraph 3.1.2. A homogeneous fibre and a coated fibre with a radius of 1 mm and a length of 10 cm have been compared while varying the absorption coefficient. The coated layer of the coated fibre is 0.05 mm thick. To absorb the same amount of photons the coated fibre must have a higher absorption coefficient than the homogeneous fibre as the path length through the dye is shorter. To make a fair comparison the fibres are therefore compared on the basis of the absorbed photons percentage. The results are depicted in figure 4.8.

For lower amount of photons absorbed, the optical efficiency and thus the concentration, is higher using the coated fibre than the homogeneous fibre. When increasing the optical density in a homogeneous fibre, more and more photons will be absorbed in an earlier stage which ultimately will act exactly the same as a coated fibre. Therefore at high absorption, the coated fibre and the homogeneous fibre approach the same

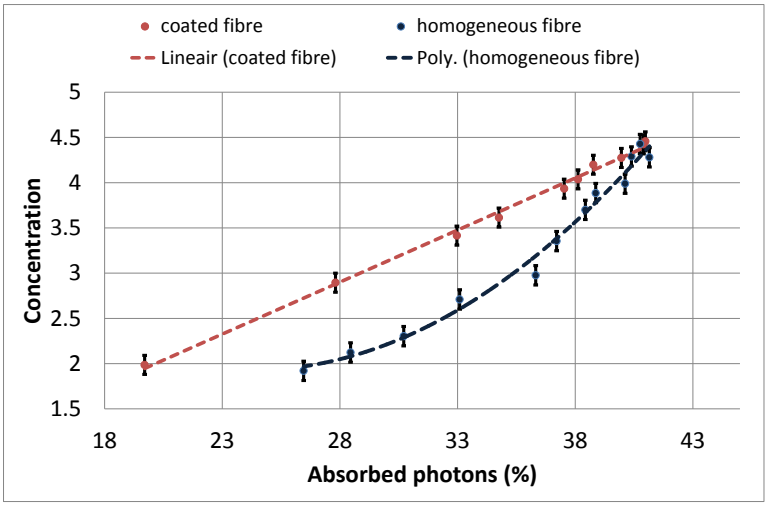

Figure 4.8: Concentration of a coated and a homogeneous fibre while varying the absorption coefficient.

concentration value. Interesting is that the trend for both configurations is eventually, when the maximum absorption is reached, the optical efficiency and thus concentration does not decrease, but remains the same value. This implies that the re-absorption losses are not increasing. As the fibre radius is small compared to the length, increasing the optical density will cause more photons to be absorbed, but when absorbed the photons have to travel a long distance to the edge of the fibre. Therefore re-absorption will take place until they are emitted with an energy that is too low to be absorbed any more. For this reason increasing the optical density will not induce a higher re-absorption loss as maximum re-absorption already takes place. Following this reasoning it is expected that increasing the length of the fibre will not decrease the optical efficiency. The geometrical concentration G will increase, resulting in higher concentration. This is investigated further in paragraph 4.2.2.

To get a better understanding of re-absorption processes and to compare these processes taking place in both fibres it has been calculated which percentage of the photons is absorbed either once, twice or three times and what the chance is to be re-absorbed. The results are depicted in figure 4.9.

The path length through the material consisting the luminescent dye is longer in the homogeneous fibre than in the coated fibre. Therefore to absorb the same amount of photons in the coated fibre, the material has to have an absorption coefficient which is higher than the absorption coefficient of the homogeneous fibre. In fact the absorption coefficient times the path length must give the same value according to the Beer Lambert law.

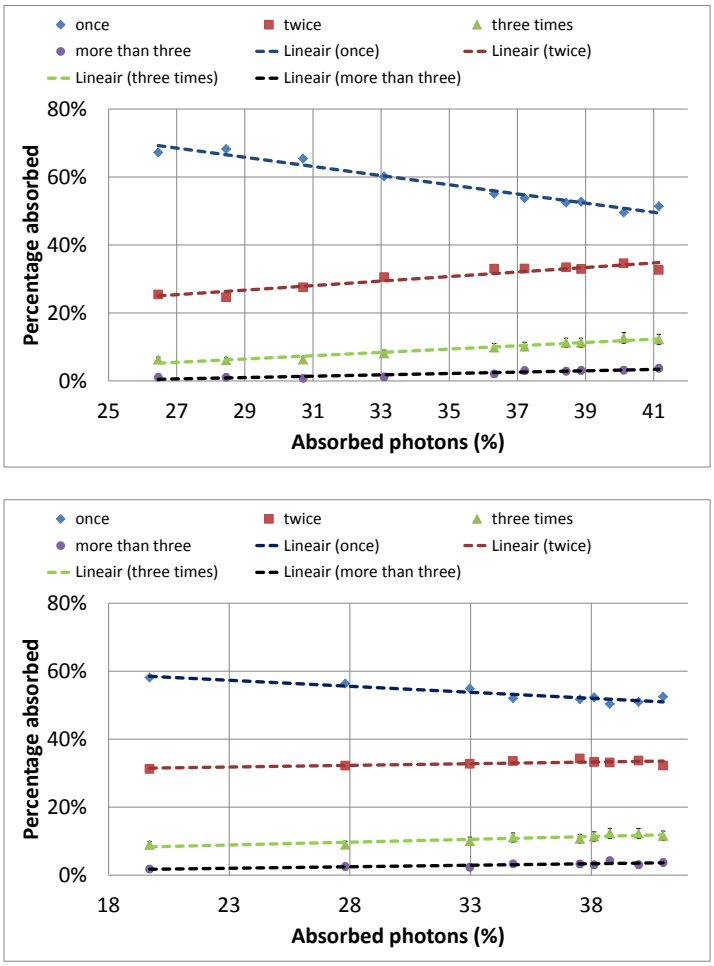

Figure 4.9: Of the photons absorbed, the percentage absorbed once, twice and three times for the homogeneous (above) and coated (below) fibre.

From the figure it can be seen that using the homogeneous fibre maximum re-absorption has not taken place at 27% photons absorbed. Increasing the optical density causes the amount of photons absorbed only once to decrease and the amount of photons absorbed twice or more to increase. When the total amount photons absorbed, depicted on the x-axis, is around 40%, maximum re-absorption has taken place.
The same trend is expected for the coated fibre, as the area where the luminescent centres are situated is inversely proportional to optical density and therefore the overall absorption should be the same. In figure 4.9 it can be seen that this is not the case. An explanation for this difference can be found in the discovery that a larger fraction of the photons emitted close to the surface are oblique rays that follow a helical path where they spiral along the hull surface of the cylinder [4]. The path length that they then have to travel to

reach the edge of the fibre is longer than when travelling almost directly.
In a coated fibre this occurs more often and therefore many photons have already reached their maximum re-absorption ability at a lower percentage absorbed photons. With this result it can also be concluded that the losses due to higher re-absorption outweigh the benefit of lower escape cone losses in a coated fibre.
In figure 4.10 the chance to be re-absorbed are depicted for respectively the homogeneous fibre and the coated fibre. In these figures it is again visible that increasing the optical density results in a higher increase in chance to be re-absorbed for the homogeneous fibre, while for the coated fibre this increase is much smaller.

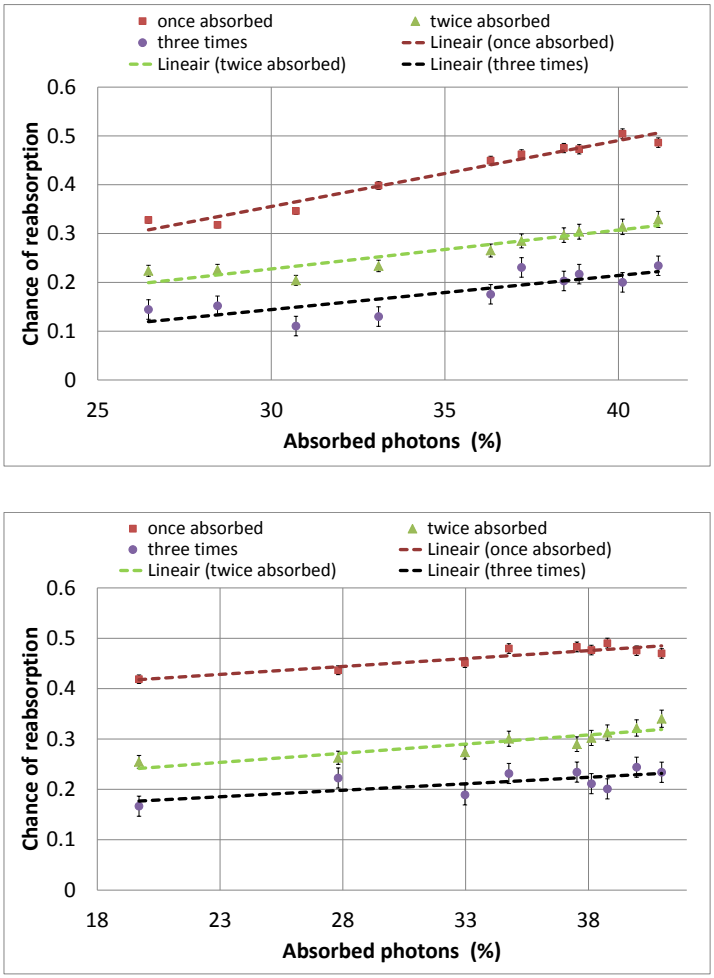

Figure 4.10: The chance to be reabsorbed after being absorbed once, twice and three time for the homogeneous (above) and coated (below) fibre.

4.2.2 Varying Length and Radius

In the last paragraph it was discussed that because the length of the fibre is long compared to the radius, the path length of photons going through the fibre is short compared to the path length of photons wave guided to the edge. This results in a high amount of re-absorption, especially at high optical density when maximum re-absorption events takes place. In other words when the photons are wave-guided to the edge of the fibre, they will have a wavelength higher than 650 nm and cannot be absorbed any more. Increasing the length of the fibre should therefore not induce more re-absorption losses. To analyse if this is the case homogeneous and coated fibres with lengths up to 1 meter have been modelled.
Similarly homogeneous fibres have been modelled with a radius of 0,5 mm and 2 mm size. If the radius is larger more photons can be absorbed when passing through the fibre but at the same time a larger radius will result in a lower geometrical concentration G.
In the figures 4.11 and 4.12 for both scenarios the concentration and optical efficiency is plotted against the size change. The concentration is the product of the optical efficiency and the geometrical concentration as described earlier. When increasing the length of the fibre from 10 cm to 40 cm, the optical efficiency

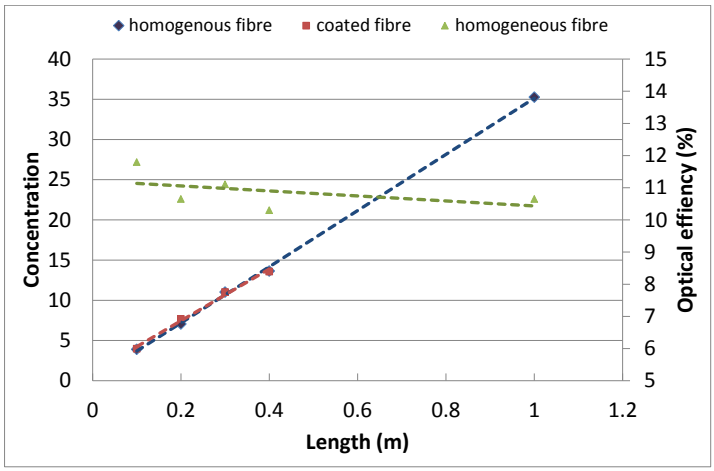

Figure 4.11: Concentration and optical efficiency of a coated and a homogeneous fibre while varying the length for incident spectrum up to 1100 nm. The amount of absorbed photons for all fibres is ∼26%, which corresponds to a absorption coefficient of 2300 m^{-1} for the homogeneous fibre and 23000 m^{-1} for the coated fibre.

decreases from 11,8 to 10,3 %. This decrease is small, which is consistent with the expectation that the re-absorption losses are minimal. Because the geometrical concentration increases from 31,8 to 127,3 the overall concentration increases severely. Continuing this trend for a homogeneous fibre with a length of 1 m

it has even been found that the overall concentration is 33,9. This result shows that using long fibres has a huge potential.

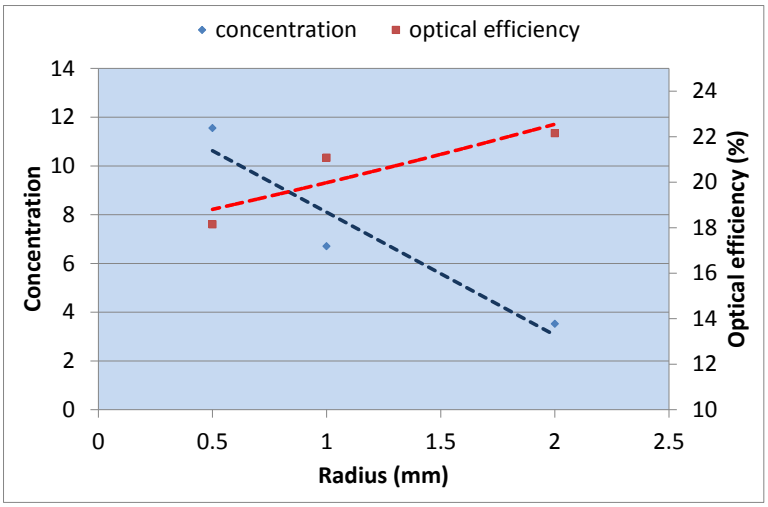

Figure 4.12: Concentration and optical efficiency of a homogeneous fibre while varying the radius size for incident spectrum up to 1100 nm. The absorption coefficient for all three fibres is 23000 m^{-1}, which corresponds to a respectively ∼35%,∼37%,∼40% absorbed for the 0.5, 1.0 and 2.0 mm radius fibres.

The optical efficiency increases from 17 to 21% when increasing the radius size of the fibre, with a length of 10 cm, from 0.5 mm to 2 mm. This increase in optical efficiency is due to an increased amount of absorbed photons as the path length crossing through the fibre is longer. This optical efficiency increase depends on the optical density of the material. If the optical density is high and maximum absorption has taken place, the radius size increase will not induce extra absorption. The photons in that case, that are not absorbed, are photons with an energy falling outside the absorption spectrum. In figure 4.12 the overall concentration decreases when changing the radius from 0,5 mm to 2 mm because the optical efficiency gain is smaller than the geometrical concentration loss.

4.2.3 Halfcoated Fibre with Mirror

Realising that the coated fibre is more efficient than the homogeneous coated fibre, the next step is to investigate if a half coated fibre or a partially coated fibre, as mentioned in paragragh 3.3, is more efficient than a coated fibre. In figure 4.13 a schematic representation of the half coated and partially coated fibre cross section is given. During the simulation it is assumed that the photons were originating from a planar source, comparable to the direct sunlight. For diffuse sunlight, the angle of the incoming photons are different and the light will not be focussed on the back side. A partially coated or a half coated fibre, is for that reason only useful for concentrating direct sunlight. It is expected that a partially coated fibre has a higher optical efficiency than a half coated fibre. The photons passing through the fibre are focussed on the back side of the fibre, allowing all photons to pass through the partially coated part of the fibre. Therefore the same amount of photons are expected to be absorbed, when the optical density is the same. Meanwhile, less of the area in the fibre is doped with organic dye, which should result in less re-absorption losses. For that reason it is expected that both fibres have a higher optical efficiency than the entirely coated fibre.

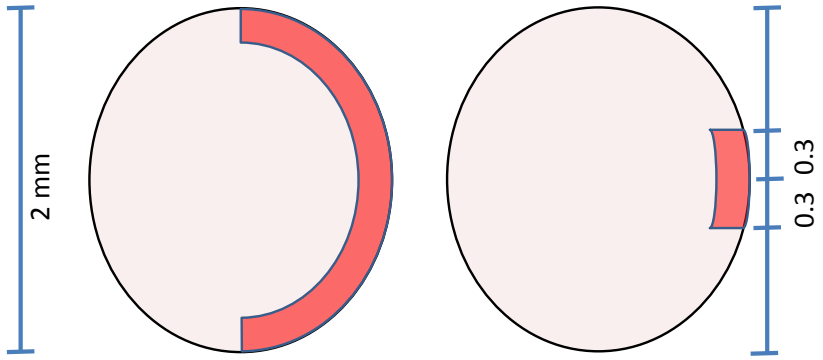

Figure 4.13: Schematic representation of the half coated (left) and partially coated (right) fibre crossection. All dimension are in mm.

In figure 4.15 it can be seen that this is in fact not the case. It is true that for the same optical density in the half coated and in the partially coated the same percentage of photons is absorbed but it is not true that the partially coated fibre is more efficient. In fact the partially coated, half coated and the normal coated are all as efficient. This is less surprising for the half coated because the decrease in area coated in inversely proportional to the increase in optical density. For the partially coated it is quite surprising though.

An explanation could be that with the optical density used, the re-absorption losses are already on their maximum level, which is coherent with the results in figure 4.9. For future research it would be interesting to repeat the same experiment but with a lower optical density.
In the same figure the results for a modelled set-up containing a half coated fibre and a mirror placed at the backside as depicted in figure 4.14 are shown. An specular and a diffuse mirror have been placed at the

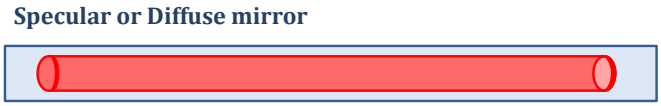

Figure 4.14: Set-up for half coated fibre with angular or specular mirror.

backside of the fibre close to the halfcoated layer. A diffuse mirror reflects with a Lambertian reflectance, while a specular mirror reflects the light with the same angle with respect to the normal of the surface. The concentration in this case has been plotted against the percentage absorption before hitting the mirror. Placing a diffuse or a specular mirror behind a half coated fibre increases the optical efficiency and thus the

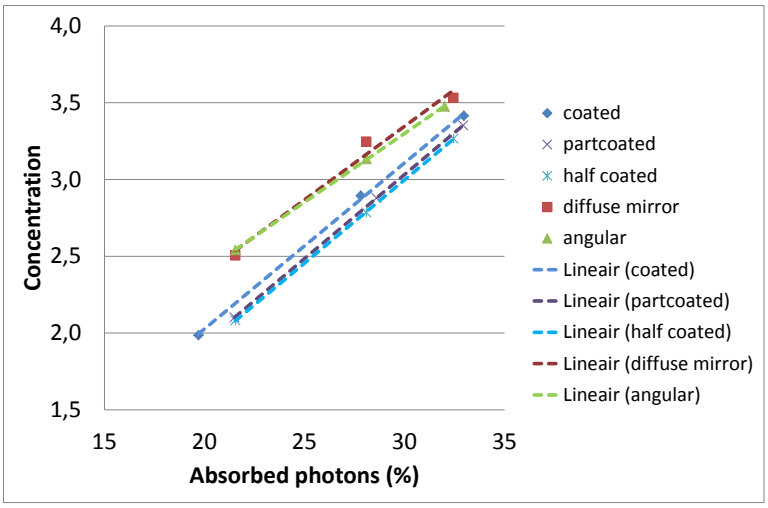

Figure 4.15: Concentration of a half coated, partially coated, coated, half coated combined with a angular mirror and half coated combined with a diffuse mirror.

concentration achieved. More photons are absorbed and therefore more photons are wave guided to the edge of fibre. A planar source of photons is simulated causing the photon beam exiting the fibre first to converge and then diverge. For that reason the increase in efficiency depends on the distance at which the specular

mirror is placed. In figure 4.15 the maximum efficiency using the specular mirror is depicted. When using the diffuse mirror the distance to the fibre does not change the results.

4.2.4 Multiple Fibres

The last configuration that has been analysed is a configuration of five coated fibres lying aligned next to each other, with a mirror placed at the back side and the source light incident on the fibre lying in the middle of the bundle. The idea is to analyse which part of the transmitted photons or photons escaped via the escape cone will be collected by neighbouring fibres. In figure 4.16 the results are shown using an angular and a diffuse mirror. It is interesting to see that the neighbouring fibres indeed can collect the photons that would be otherwise lost and therefore an array of fibres gives a slightly higher optical efficiency than is achieved for isolated photons. If all the fibres would be exposed to sunlight then their optical efficiency would increase with $\sim$1% from their direct neighbouring fibres and $\sim 0,1\%$from fibres lying one fibre away.

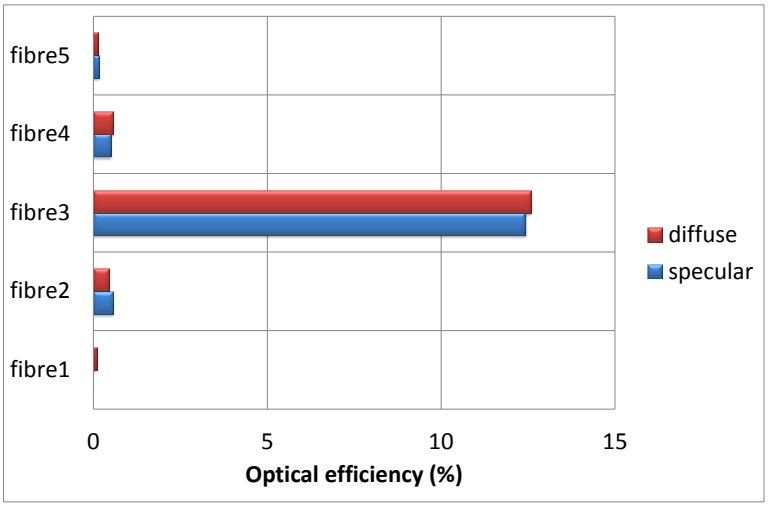

Figure 4.16: Optical efficiency increase for neighbouring fibres.

4.3 Summary

The ray tracing model PVtrace has been used to simulate the concentrating potential of LSC fibres. First the optical efficiency of four homogeneous fibres calculated by the model are compared to experimentally found values. When using the solar simulator to excite the lumogen red electrons the results are not in good agreement possibly due to uncertainty of the solar simulator spectrum shape but when using the laser as

source the results are more similar to each other. The modelled and experimental results are in each others error bar range and therefore it can be used to predict the potential of other LSC fibres. An explanation for the difference in the results might be found in a lower LQY of the dye when imbedded in a polymer, like PMMA.

A homogeneous fibre, coated fibre, half coated fibre, partially coated fibre and multiple coated fibres have been modelled. In addition the length and radius size have been varied and mirrors have been added to the set-up. Comparing the different configurations is it found that the coated fibre has a higher optical efficiency than the homogeneous fibre. Although more re-absorption takes place in a coated fibre, the escape cone losses are lower resulting in an overall more efficient wave guiding. Depending on the absorption coefficient of the material the radius can be increased to ensure maximum absorption of incoming photons. Increasing the radius however, results in a lower geometrical concentration value which decreases the overall concentration. This can be compensated by increasing the length. After a certain length, depending on the absorption coefficient, making a larger fibre will not result in more re-absorption as maximum re-absorption has already taken place. The only loss that then occurs is host absorption. For that reason it can be very beneficial to produce long fibre LSC because the geometrical concentration increase is higher than the optical efficiency drop.

For the same amount of photons absorbed the partially coated fibre and the half coated fibre have exactly the same optical efficiency as the coated fibre. It was expected that the partially coated fibre would experience less re-absorption losses and therefore be more efficient but it could be that with the set-up used the absorption coefficient was too high to see this effect. Including either an angular or diffuse mirror to the half coated fibre set-up increased the optical efficiency with $\sim$2%. Placing fibres side by side in configuration with a mirror does increase the optical efficiency as transmitted photons and photons lost through the escape cone can be collected by the neighbouring fibres.

It can be concluded that high concentration is possible when using fibre LSCs, especially when using long coated fibres. Using fibres will induce high re-absorption losses as the length that the photons have to travel to the edge is relatively far. This is compensated by the high geometrical concentration of this configuration and therefore it is not a large issue when maximum re-absorption takes place. Maximising the geometrical concentration by tuning the length and the radius and reducing the escape cone losses by placing the dye close to the surface are characteristics that play the most important role when applying an LSC fibre to concentrate the sunlight.

Chapter 5

Spectral Modelling

Luminescent solar concentrators are particularly suitable in urban areas where a larger part of the sunlight is scattered due to aerosol pollutants and reflected by the surfaces of buildings. This diffuse light can be collected by the LSC as well as the direct light. In this chapter the contribution of diffuse light collection by the fibre LSC is compared to the direct light contribution. The programme SMARTS 2.9.5 developed by the national renewable energy laboratory (NREL) [7][8] is used to model clear sky diffuse and direct spectra in London on the 22nd of December 2011 and the 21st of June 2011 for every hour of the day. The data is converted to photon flux per wavelength and used as source spectrum data in PVtrace. The optical efficiency of a homogeneous fibre during a summer and a winter day for the diffuse and the direct spectrum is simulated. The aim is to research what realistically the concentration potential of a LSC fibre in connected to a silicon and Galium arsenide solar cell in London is and how the diffuse and the direct spectrum contribute to it.

5.1 Set-up

5.1.1 SMARTS data

Smarts models clear sky spectral irradiation throughout the year and on every location on the earth. Changes is the atmosphere affect the photon flux per wavelength which SMARTS predicts. In the input file used it is assumed that the fibre LSC was located on a concrete surface in an urban environment at the latitude at longitude coordinates [51, 0] of London. The exact input file used can be found in the Appendix E. Note that only clear sky spectra are modelled and that on a cloudy day more light would be scattered, contributing to a larger diffuse spectrum and a smaller direct spectrum.

5.1.2 PVtrace set-up

A homogeneous fibre with a radius size of 1 mm and a length of 10 cm and a peak absorption coefficient of 6400 m^{-1} was modelled. To model the diffuse light and the direct light realistically the angle of incidence was taken into account. For the diffuse light, originating from all directions, a source of 20 cm by 10 cm, was placed 2 mm above the fibre. In this way the simulated fibre was hit by photons with a broad angle incidence as well a narrow angle incidence. The size of the source and the distance to the fibre is chosen in such a way that 95% of the photons with the broadest angle are reflected when hitting the fibre. Only the photons that hit the fibre are counted.
For the direct spectrum, the calculations made in paragraph 3.1.1 are used. The fibre is placed along the North-South axis and the cosine of the angle between this axis and the ray of the sun is $\cos\beta = \cos\alpha \cos A$ where α is the solar altitude angle and A the solar zenith angle. The values of these angles have been calculated by SMARTS for each hour and can be found in Appendix G.

5.2 Results

For each hour on the 21st of June and the 22nd of December the amount of photons collected originating from the direct and from the diffuse spectrum has been calculated. The results are depicted in figure 5.2 and 5.1.

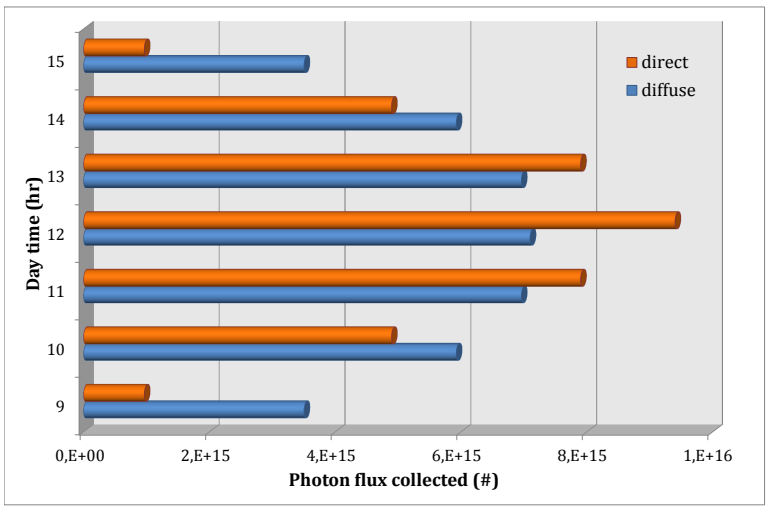

Figure 5.1: Photons collected and wave guided to the edge, by the homogeneous fibre lying North-South on the 22nd of December 2011

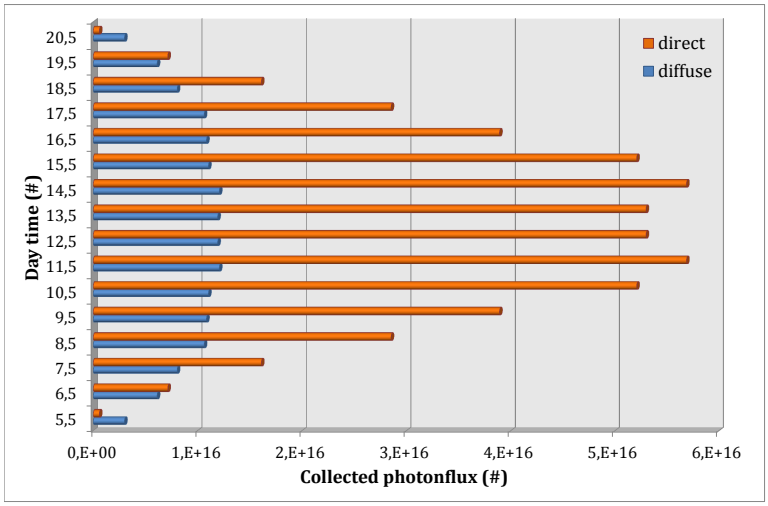

Figure 5.2: Photons collected and wave guided to the edge, by the homogeneous fibre lying North-South on the 21st of June 2011.

In the first figure it can be seen that in the winter the diffuse has a larger contribution at the beginning and end of the day, while the direct spectrum has a larger contribution during noon. Overall the contributions of the diffuse spectrum and the direct are quite similar and therefore it can be concluded that the diffuse light as well as the direct light in the winter in London play an important role in fibre LSC applications.
In the summer the direct spectrum contains more photons and the optical efficiency is higher because the angle between the incoming rays and the surface normal is less broad. This results in a higher amount of photons collected originating directly from the sun. The collected diffuse photons increase as well in the summer due to an increase in photon flux but much less than the increase in direct photon collection. This leads to significantly larger direct spectrum contribution to the overall collection in the summer. Surprisingly, the direct photon collection is not the highest at the middle of the day. Even though the photon flux is higher at that time of the day, the angle of incidence is broader causing more reflection to take place.
Perhaps more interesting is to analyse what the optical efficiency is and what the concentrating potential is with respect to the silicon and Galium arsenide band gap. The optical efficiency depends on the spectrum range that is taken in to account, especially for the direct spectrum this is the case. In figure 5.5 and 5.6 the direct and the diffuse spectra throughout the day on the 22nd of December are depicted. A substantial part of the direct spectrum has a wavelength larger than 800 nm as can be seen in figure 5.5 which will not be absorbed by the lumogen red dye and is lost. The diffuse spectrum has a different shape and is mainly apparent between 300 and 800 nm, which can be absorbed by the dye.
The percentage of the whole spectrum that can be absorbed by the lumogen red dye and of the spectrum

up to the silicon band gap for the two days and for the direct and the diffuse can be found in Appendix E. Other organic dyes, or even a mixture of organic dyes, with a different absorption range can be used as luminescent material to match the solar spectrum and the band gap of the solar cell used. For all the different spectra modelled by SMARTS the average photon energy (APE) is calculated and can be found in the appendix ref H

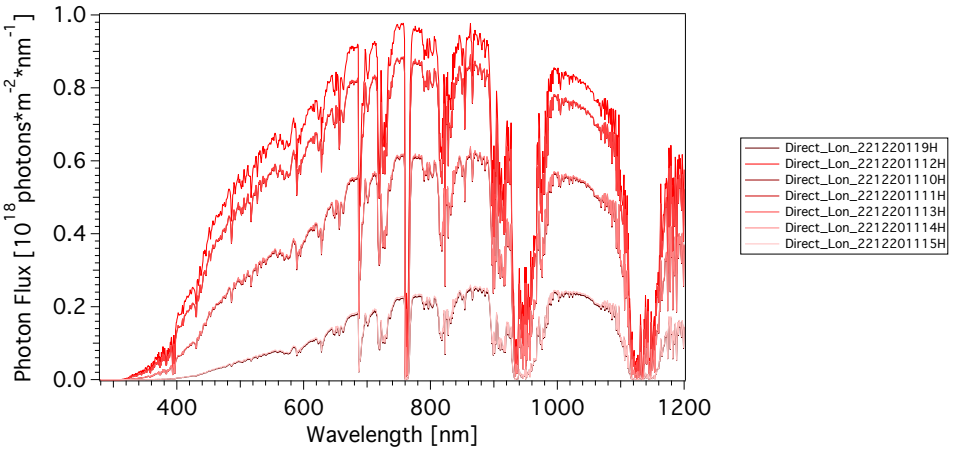

Figure 5.3: Direct spectrum throughout the day on the 22nd of December 2012

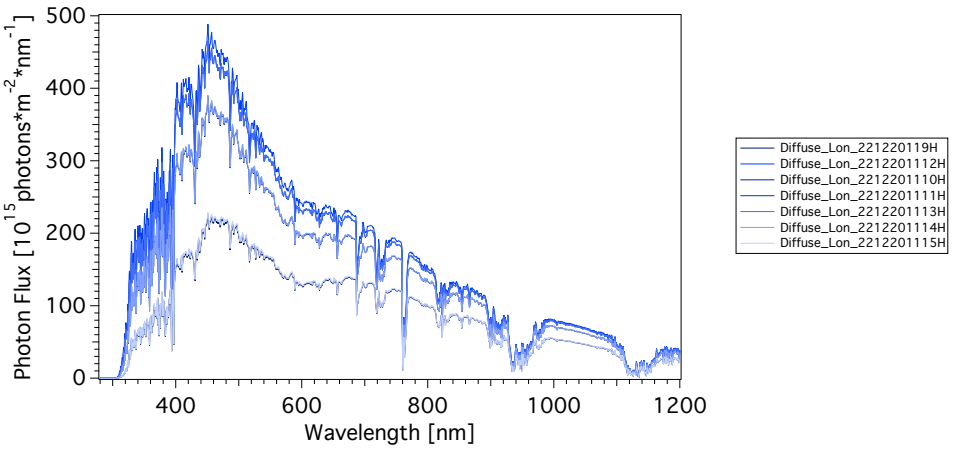

Figure 5.4: Diffuse spectrum throughout the day on the 22nd of December 2012.

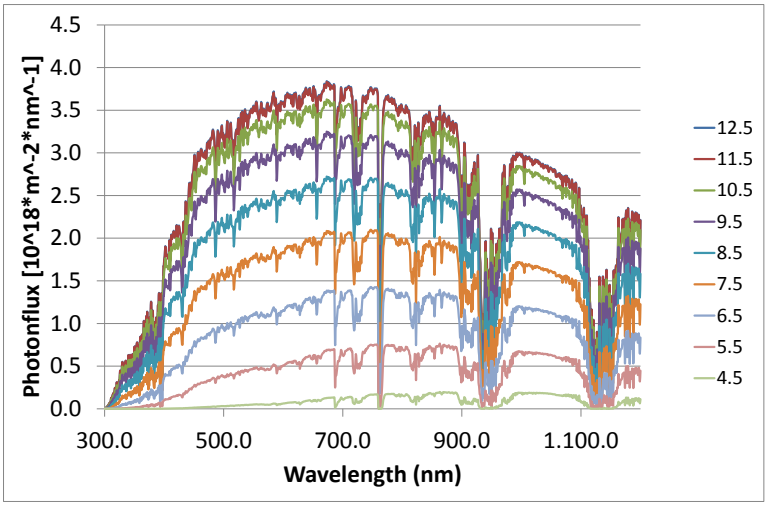

Figure 5.5: Direct spectrum throughout the morning on the 21st of June 2011. The spectra in the afternoon have the same shape as in the morning

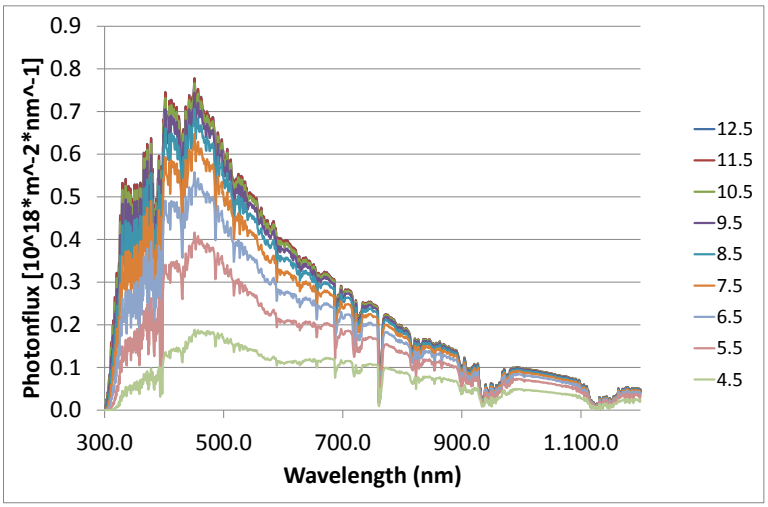

Figure 5.6: Diffuse spectrum throughout the morning on the 21st of June 2011. The spectra in the afternoon have the same shape as in the morning.

The average optical efficiency is calculated, weighted for the amount of photons collected, compared to the whole spectrum (up to 4000 nm), to the silicon band gap (up to 1100 nm) and to the Galium arsenide band gap (up to 843 nm). The effective concentration factor of the LSC fibre attached to the two cells are calculated, compared to the amount of useful photons for these solar cells. The concentration factor with respect to the whole spectrum is calculated as well. All results can be found in the table 5.1.

Table 5.1: Comparing the optical efficiency and concentration performance of lumogen red fibre LSC connected to a silicon cell and a to Galium arsenide cell. The optical efficiency and concentration of the fibre LSC are also shown with respect to the whole spectrum.

	Optical efficiency	Concentration
Spectrum up to 4000 nm		
Summer diffuse	0.23	7.26
Summer direct	0.08	2.48
Winter diffuse	0.21	6.72
Winter direct	0.05	1.66
Silicon cell spectrum		
Summer diffuse	0.25	7.83
Summer direct	0.12	3.84
Winter diffuse	0.21	6.80
Winter direct	0.09	2.86
Galium arsenide cell spectrum		
Summer diffuse	0.27	8.64
Summer direct	0.16	5.12
Winter diffuse	0.26	8.34
Winter direct	0.14	4.36

From the results we can conclude that in an urban environment the fibre LSC works very well as a concentrator. The fibre in combination with the silicon solar cell has the ability to concentrate the direct light ~ 3 times and the diffuse light ~ 7 times. This shows that the fibre LSC has a high potential to decrease the cost of photovoltaic electricity production. When using the lumogen red dye as luminescent material it is best to combine the LSC with a solar cell that has a band gap of 1.55 eV which corresponds to the wavelength of the photons emitted. In that case maximum use of the energy of the collected photons takes place.

Galium arsenide fits this profile quite well and therefore will produce a higher power than the silicon solar cell. Also the concentration compared to the photons that are collected by the cell without the fibre is higher, namely ~ 4.5 for the direct and ~ 8.5 for the diffuse. Luminescent species emitting in the 900-1000 nm range would be more suitable to use in combination with the silicon solar cell.

5.3 Summary

The diffuse and the direct spectra for the 21st of June 2011 and the 22nd of December 2012 during the day, have been modelled and used as source input in PVtrace. During the simulation the angle of incidence is also taken in to account. In the winter the diffuse spectrum delivers a higher contribution in the beginning and at the end of the day and overall the amount of photons collected coming from the diffuse are quite similar to the amount of photons coming from the direct spectrum. In the summer the photon flux originating from direct spectrum is higher and the angle between the rays and the fibre less steep resulting in $\sim$5 times as many photons collected. The diffuse spectrum photon flux also increases but much less than the direct spectrum photon flux.

The spectra of the diffuse and the direct light show that these results found depend on the band gap of the solar cell and the emission spectrum of the luminescent centre. The diffuse light is mainly apparent between 300-800 nm and can be absorbed by the lumogen red dye well while the direct spectrum contains a substantial part of photons with a wavelength higher than 800 nm.

The Galium arsenide solar cell, with a band gap of 1.49 eV, matches the lumogen red dye emission spectrum well. Combining the LSC fibre with a gallium arsenide solar cell has the potential to effectively concentrate direct light ~ 4.5 times and the diffuse light ~ 8.5 times.

Chapter 6

Summary and Conclusion

The potential of using a luminescent solar concentrator with a fibre geometry has been investigated by means of a theoretical comparison of the optical concentration with the conventional planar LSC, modelling the optical efficiency with PVtrace and quantifying the performance when applied in the urban environment of London. Three loss mechanisms in the LSC depend on the geometry of the LSC: host absorption loss, escape cone loss and reflection loss. All these losses are larger in the fibre LSC than in the plane LSC but are small compared to the larger geometrical concentration of the fibre LSC. Taking the three loss mechanisms and the geometrical concentration factor into account when, comparing the fibre and the plate LSC with the same volume, the same collection area, host absorption of 0.1 m^{-1} and a refractive index of 1.5 shows that the fibre or in general cylinder has a optical concentration which can be 1.5 times as large as that of the plate.

To calculate the host absorption loss of both geometries the calculation performed by McIntosh (2007) were followed. These calculation account for r=0 and r=R. For future research it would be interesting to analyse how the host absorption changes with r. This loss is small compared to the other losses when the host absorption is 0.1 m^{-1} and therefore it will probably not affect the result a lot but when the host absorption is higher understanding how the path of the emitted photon changes with respect to r is important. It is already known that photons emitted close to the surface have a larger chance to follow a helical path but it would be interesting to extend this theory.

The trapping efficiency of the cylinder depends on the position of the emission point with respect to r in contrast to the trapping efficiency of the plate where it does not depend on the location of the emission point. The closer the emission point is to the surface, the larger is the chance that the photon sees total internal reflection. For this reason a polymer fibre coated with an organic dye is expected to experience a larger trapping efficiency than a homogeneous organic dye doped polymer fibre. The calculated photon path

through the fibre shows that the convex surface of the fibre induces a focusing of the rays. An interesting configuration to analyse is therefore a fibre with a partially coated layer at the side where the rays are focussed.

The ray tracing model PVtrace has been used to increase our understanding of the working mechanisms in the fibre LSC and to optimise the optical concentration that the fibre can achieve. Experimental research was first performed on four homogeneous fibres with radius size varying between 0.25 mm and 1 mm and length varying between 10 cm and 20 cm to verify the results of the model. A 473 nm laser and a solar simulator was used as source during the experiments. The optical efficiency results when using the laser as a source were in enough agreement with the PVtrace results and therefore the model could be used for further tests. A large uncertainty in the emission spectrum of the solar simulator and in the LQY of the dye incorporated in PMMA, resulted in some unconsistency in the modelled and experimental results. For future research it would be interesting to repeat this measurement when the emission spectrum and LQY is well known.

The coated fibre has a larger optical efficiency than the homogeneous fibre for the same amount of photons absorbed according to the PVtrace results. For both fibres the optical efficiency increases when increasing the absorption coefficient until the maximum absorption is reached and the optical efficiency plateaus. Due to a larger fraction photons emitted with a helical path in the coated fibre more re-absorption takes place in this configuration. The absorption coefficient cannot be increased limitlessly and is restricted to the solubility of the luminescent material in the host matrix. A higher absorption coefficient is needed to achieve the same amount of photons absorbed in the coated fibre as the path length through the luminescent material is smaller. Interesting is to research what the maximum absorption is for both configurations and then compare the optical efficiencies. It could be that even though the trapping efficiency is higher when using the coated fibre, the homogeneous fibre has a larger potential because more photons can be absorbed.

When the absorption coefficient is high and many photons are absorbed, maximum re-absorption takes place because the path length through the fibre is short compared to the path length from the point of emission to the edge of the fibre. Therefore increasing the length of the fibre does not induce more re-absorption but it does increase the geometrical concentration. The results attained with PVtrace show that the increase in geometrical concentration is larger than the loss due to host absorption, with an absorption coefficient of 0.3 m^{-1} assumed. This means that increasing the length of the fibre has the potential to increase the optical concentration without a limit.

Changing the radius of the fibre causes the path length of the photons going through the fibre to be longer and therefore the percentage absorbed to increase but at the same time the geometrical concentration to decrease. The best approach when designing an LSC fibre is probably to first investigate the maximum optical density possible depending on the material characteristics, then increasing the radius until the path

length is long enough for maximum absorption to take place and finally increasing then the length in such a way that there is a high geometrical concentration.

The partial coated fibre and the half coated fibre did not increase the optical efficiency when compared to the coated fibre. This can be explained by the long path length of the photon when emitted close to the surface which brings maximum re-absorption along with it. Perhaps when comparing the configurations with a lower optical density the difference will be more apparent. Important is to note that with the partially coated and the half coated fibre the path length through the luminescent material when passing through the fibre is even smaller than when using a coated fibre and therefore to achieve the same amount of absorption an even higher optical density must be applied. Or in other words when using the same material less photons are absorbed in the half coated fibre and partially coated fibre than in the coated fibre which limits the optical efficiency.

Aligning multiple fibres in a row combined with a specular or a diffuse mirror shows that photons reflected or transmitted through one fibre can be collected by the other fibres. This could be another approach instead of increasing the radius size to increase the percentage absorbed when the optical density is at maximum value.

The diffuse and the direct spectrum have been modelled for the 22nd of December and the 21st of June for every hour by the programme SMARTS and used as source in PVtrace. Using a fibre LSC of 1 mm radius size and 10 cm length to concentrate the light falling on a Gallium arsenide solar cell can result in ~ 4.5 times as much direct light collected and around ~ 8.5 times as much diffuse light collected. This result shows that applying the LSC fibre in urban areas has a huge potential. There is still a lot of research to be done in this field as in this research only one location on two days for one type of organic dye and two types of solar cells have been investigated. All these inputs can be varied and it would be very interesting to see whether these results are also applicable at other locations and to match the type of dye to the type of solar cell to the global spectrum collected.

Appendix A

Reflection

Table A.1: Reflection coefficient for a fibre and a flat plate LSC

time (hr)	plate 0°	plate, 52°	plate 52°	n-s fibre	e-w fibre	fibre 52°	photons(#/m^2)
			Winter				
9	0,58	0,06	0,05	0,16	0,17	0,15	1,70E+020
10	0,36	0,04	0,04	0,16	0,17	0,14	4,82813E+20
11	0,27	0,04	0,04	0,19	0,15	0,15	7,15368E+20
12	0,25	0,04	0,04	0,19	0,16	0,14	7,15E+020
13	0,27	0,04	0,04	0,19	0,15	0,15	7,15368E+20
14	0,36	0,04	0,04	0,16	0,17	0,14	4,82813E+20
15	0,58	0,06	0,05	0,16	0,17	0,15	1,70051E+20
average	0,32	0,04	0,04	0,18	0,16	0,14	3,45E+021
weighted average	0,37	0,05	0,04	0,18	0,16	0,14	
			Summer				
5,5	0,61	1,00	1,00	0,18	0,16	0,15	1,29E+020
6,5	0,27	1,00	1,00	0,15	0,25	0,15	6,05822E+20
7,5	0,15	0,56	1,00	0,14	0,27	0,15	1,2253E+21
8,5	0,08	0,17	0,92	0,14	0,14	0,18	1,87587E+21
9,5	0,06	0,08	0,40	0,14	0,15	0,15	2,48523E+21
10,5	0,05	0,05	0,21	0,14	0,16	0,15	2,99671E+21
11,5	0,04	0,04	0,13	0,15	0,14	0,15	3,36774E+21
12,5	0,04	0,04	0,11	0,15	0,14	0,15	3,5672E+21
13,5	0,04	0,04	0,11	0,15	0,14	0,15	3,5672E+21
14,5	0,04	0,04	0,13	0,15	0,14	0,15	3,36774E+21
15,5	0,05	0,05	0,21	0,14	0,16	0,15	2,99671E+21
16,5	0,06	0,08	0,40	0,14	0,15	0,15	2,48523E+21
17,5	0,08	0,17	0,92	0,14	0,14	0,18	1,87587E+21
18,5	0,15	0,56	1,00	0,14	0,27	0,15	1,2253E+21
19,5	0,27	1,00	1,00	0,15	0,25	0,15	6,05822E+20
20,5	0,61	1,00	1,00	0,18	0,16	0,15	1,29365E+20
average	0,07	0,15	0,38	0,15	0,16	0,15	3,25E+022
weighted average	0,16	0,37	0,59	0,15	0,18	0,15	
total photons lost	3,40E+21	4,91E+21	1,24E+22	5,36E+21	5,79E+21	5,43E+21	
total weighted average	0,0945	0,1366	0,3436	0,1491	0,1611	0,1510	

Appendix B

Trapping Efficiency of a Cylinder

This chapter is written with assistance of Luca Patrignani.

B.1 Derivation of Eq. 3.4

By plugging $x^2 + (y+r)^2 = R^2$ into the scalar product equation (i.e. into the third equation of 3.3), we have

$$\frac{R^2 - yr - r^2}{R\sqrt{R^2 - 2yr - r^2 + z^2}} = \sqrt{1 - \frac{1}{n^2}} \Rightarrow \frac{R - y\frac{r}{R} - \frac{r^2}{R}}{\sqrt{R^2 - 2yr - r^2 + z^2}} = \sqrt{1 - \frac{1}{n^2}}$$

We can now take all the square roots on the right side, and square the both sides. This gives

$$R^2 + y^2\frac{r^2}{R^2} + \frac{r^4}{R^2} - 2ry - 2r^2 + 2y\frac{r^3}{R^2} = (1 - 1/n^2)(R^2 - 2yr - r^2 + z^2)$$

If we take all on the left and multiply times R^2/r^2, we have

$$y^2 - 2r\cancel{\frac{R^2}{r^2}}y + 2ry - 2R^2 + r^2 + R^2\frac{R^2}{r^2} + 2r\frac{R^2}{r^2}\left(\cancel{1} - \frac{1}{n^2}\right)y - \frac{R^2}{r^2}\left(1 - \frac{1}{n^2}\right)(R^2 - r^2 + z^2) = 0$$

were we explicitly wrote the y terms separately in order to cancel out the ones that simplify. By setting $\rho = r/R$, we now have

$$y^2 - 2R\left(\frac{1}{n^2\rho} - \rho\right)y + R^2\left(\frac{1}{\rho^2} + \rho^2 - 2\right) - \frac{1}{\rho^2}\left(1 - \frac{1}{n^2}\right)(R^2 - \rho^2R^2 + z^2) = 0 \tag{B.1}$$

This has solutions

$$y = R\left(\frac{1}{n^2\rho} - \rho\right) + \pm\sqrt{R^2\left(\frac{1}{n^2\rho} - \rho\right)^2 - R^2\left(\frac{1}{\rho^2} + \rho^2 - 2\right) + \frac{1}{\rho^2}\left(1 - \frac{1}{n^2}\right)(R^2 - \rho^2R^2 + z^2)}$$

The bit under square root can be rearranged by factorizing R^2/ρ^2 . So we can finally write

$$y = \frac{R}{\rho}\left[\frac{1}{n^2} - \rho^2 \pm \sqrt{\left(1-\frac{1}{n^2}\right)\left(\rho^2 - \frac{1}{n^2} + \frac{z^2}{R^2}\right)}\right] \tag{B.2}$$

Since $x = \pm\sqrt{R^2-(y+r)^2}$, we immediately have

$$x = \pm\sqrt{R^2 - \frac{R^2}{\rho^2}\left[\frac{1}{n^4} + \left(1-\frac{1}{n^2}\right)\left(\rho^2 - \frac{1}{n^2} + \frac{z^2}{R^2}\right) \pm \frac{2}{n^2}\sqrt{\left(1-\frac{1}{n^2}\right)\left(\rho^2 - \frac{1}{n^2} + \frac{z^2}{R^2}\right)}\right]}$$

If we factorize the term $R^2/(n^2\rho^2)$, forgetting for now about the second square root, we can rearrange the other terms as

$$\cancel{n^2\rho^2} - \frac{1}{n^2} - \cancel{n^2\rho^2} + 1 - \frac{z^2n^2}{R^2} + \rho^2 - \frac{1}{n^2} + \frac{z^2}{R^2} = \rho^2 + 1 - \frac{2}{n^2} - \frac{z^2}{R^2}(n^2-1)$$

We can now write the solution for x as

$$x = \pm\frac{R}{n\rho}\sqrt{\rho^2 + 1 - \frac{2}{n^2} - \frac{z^2}{R^2}(n^2-1) \mp 2\sqrt{\left(1-\frac{1}{n^2}\right)\left(\rho^2 - \frac{1}{n^2} + \frac{z^2}{R^2}\right)}} \tag{B.3}$$

The condition on z for having real solutions comes from setting the argument of the square root ≥ 0. If we look at the solution for y, this holds

$$\rho^2 - \frac{1}{n^2} + \frac{z^2}{R^2} \geq 0 \tag{B.4}$$

from which Eq. 3.5 is immediately deduced.

We could carry out a similar analysis for the argument of the main square root in the solution for x, but this will not be treated here.

B.2 Derivation of Eq. 3.6

The cartesian coordinates can be written as

$$\begin{cases} x = \wp\sin\theta\sin\phi \\ y = \wp\sin\theta\cos\phi \\ z = \wp\cos\theta \end{cases} \tag{B.5}$$

. Using Eq. B.5,we can write the equation $x^2 + (y+r)^2 = R^2$ as

$$x^2 + y^2 + 2ry + r^2 = R^2 \quad \Rightarrow \quad \wp^2\sin^2\theta + 2r\wp\sin\theta\cos\phi + r^2 = R^2$$

$$\Rightarrow \wp^2 + 2r\wp\frac{\cos\phi}{\sin\theta} + \frac{r^2-R^2}{\sin^2\theta} = 0$$

This has solution

$$\wp = -r\frac{\cos\phi}{\sin\theta} \pm \sqrt{r^2\frac{\cos^2\phi}{\sin^2\theta} + \frac{R^2-r^2}{\sin^2\theta}}$$
$$\Rightarrow \wp = \frac{1}{\sin\theta}(-r\cos\phi \pm \sqrt{R^2 - r^2 + r^2\cos^2\phi})$$

Since $\wp$ has to be positive, the + solution is the only one acceptable. So finally

$$\wp = \frac{R}{\sin\theta}(\sqrt{1-\rho^2+\rho^2\cos^2\phi} - \rho\cos\phi)$$

This result can be used to write y and z as functions of θ and ϕ. From Eq. B.5 it is straightforward that

$$y = R\cos\phi(\sqrt{1-\rho^2+\rho^2\cos^2\phi} - \rho\cos\phi) \tag{B.6}$$

$$z = \frac{R}{\tan\theta}(\sqrt{1-\rho^2+\rho^2\cos^2\phi} - \rho\cos\phi) \tag{B.7}$$

We can now take Eq. B.1, substitute y and z with the expressions found in Eq. B.6 and B.7, and solve for $\cos\phi = F(n,\rho,\theta)$. From this point onward, we will not present every single step like we did in Sec. B.1, as this calculation is much longer.

After the substitutions, rearranging the terms as powers of $\cos\phi$ and taking the terms containing $\sqrt{1-\rho^2+\rho^2\cos^2\phi}$ on the right, we have

$$2\rho^2\cos^4\phi + \cos^2\phi\left[1+\frac{2}{n^2} - 3\rho^2 - \left(1-\frac{1}{n^2}\right)\frac{2}{\tan^2\theta}\right] +$$
$$+\left(1-\frac{1}{\rho^2}\right)\left[\frac{1}{n^2} - \rho^2 - \left(1-\frac{1}{n^2}\right)\frac{1}{\tan^2\theta}\right] =$$
$$= \left\{2\rho\cos^3\phi + \frac{2}{\rho}\cos\phi\left[\frac{1}{n^2} - \rho^2 - \left(1-\frac{1}{n^2}\right)\frac{1}{\tan^2\theta}\right]\right\}\cdot\sqrt{1-\rho^2+\rho^2\cos^2\phi}$$

If we set

$$c = \frac{1}{n^2} - \rho^2 - \left(1-\frac{1}{n^2}\right)\frac{1}{\tan^2\theta}$$

we can write this equation in a more manageable fashion, obtaining

$$2\rho^2\cos^4\phi + \cos^2\phi(1+2c-\rho^2) - \left(1-\frac{1}{\rho^2}\right)c = \left(2\rho\cos^3\phi + \frac{2c}{\rho}\cos\phi\right)\sqrt{1-\rho^2+\rho^2\cos^2\phi}$$

By squaring both sides[1], the 8^{th} and 6^{th} power terms cancel out, and we are left with

$$\cos^4\phi + \frac{2c}{\rho^2}\cos^2\phi + \frac{c^2}{\rho^4} = 0$$

which has the positive solution

$$\cos\phi = \sqrt{-\frac{c}{\rho^2}} \tag{B.8}$$

Eq. 3.6 is just Eq. B.8 where c has been explicitly written in terms of n, ρ and θ.

[1] As a remark, it is important to remember that squaring could add solutions which are in fact not acceptable. In the end, limiting θ and ϕ to be within the range $[0;\pi/2]$ will allow to restrict the solutions and discard the unwanted ones.

Appendix C

Path length Calculation

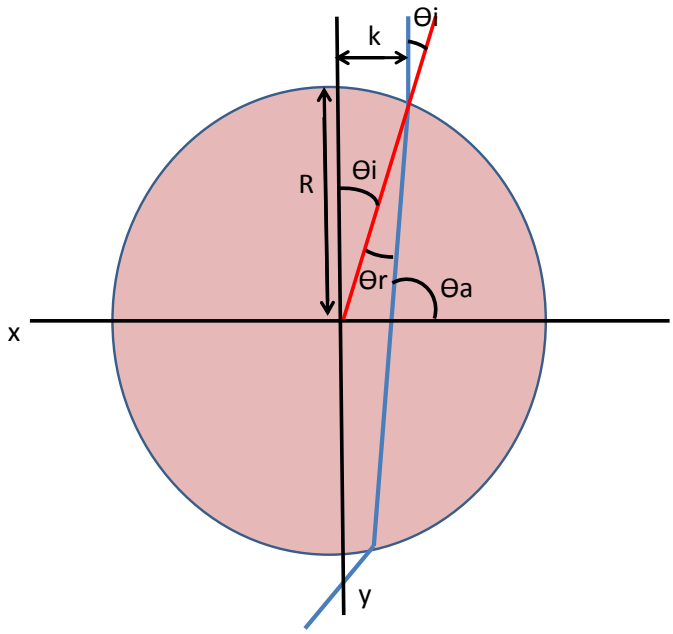

Figure C.1: Cross section of the fibre with normal incident light (blue line) passing through.

In the figure, the angle of incidence, θ_i, angle of refraction, θ_r of light incident on the fibre orginating from a planar source lying parallel to the fibres axis. The angle that the incident light has with the x axis is defined as θ_a. This angle can be used to calculate the lights slope when passing though the fibre. The distance between the incoming light and the y axis is defined as k, the refractive index as n and the radius is defined as R. With these parameters the three angles can be calculated as follows:

$\theta_i = \sin^{-1}(k)$, $\theta_r = \sin^{-1}(\sin(\theta_i/n)$ and $\theta_a = 0.5\pi - \theta_i + \theta_r$

. The slope of the line that the incident light follows when travelling through the fibre is equal to $\tan(\theta_a)$. Knowing that the line travel through point $[k,\sqrt{k^2 + R^2}]$, the equation of the line in the form of y=ax+b can be calculated. The distance that the photon has travelled through the fibre can by calculated by finding the second point where the line intersects with the fibre axis. This is done by setting the line equation equal to the cirkel equation $y = \sqrt{k^2 + R^2}$. Solving this gives for every distance k a solution for the pathlength. The results can be found in table C.1.

Table C.1: θ_i, θ_r, the slope a and the pathlength of a photon incident with a distance k from the y-axis, following figure C.1

k	θ_i	θ_r	a	pathlength
0.1	0.100	0.067	29.883	1.932
0.2	0.201	0.134	14.765	1.863
0.3	0.305	0.201	9.643	1.792
0.4	0.412	0.270	7.016	1.719
0.5	0.524	0.340	5.380	1.644
0.6	0.644	0.412	4.233	1.567
0.7	0.775	0.486	3.353	1.490
0.8	0.927	0.563	2.619	1.419
0.9	1.120	0.644	1.938	1.379
1	1.571	0.730	0.894	1.541
average				1.63

Appendix D

Absorption data

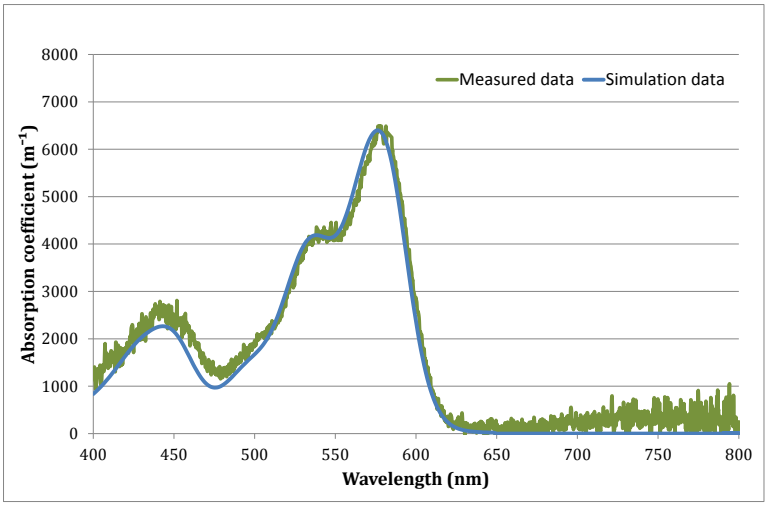

Figure D.1: Absorption spectrum of the fibre with a radius of 0.5 mm measured and used for the simulation with PVtrace

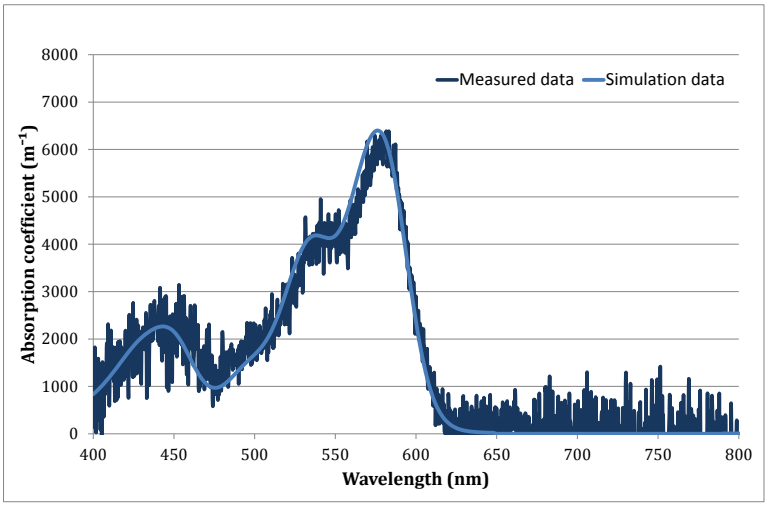

Figure D.2: Absorption spectrum of the fibre with a radius of 0.25 mm measured and used for the simulation with PVtrace

Appendix E

Solar Simulator Spectrum

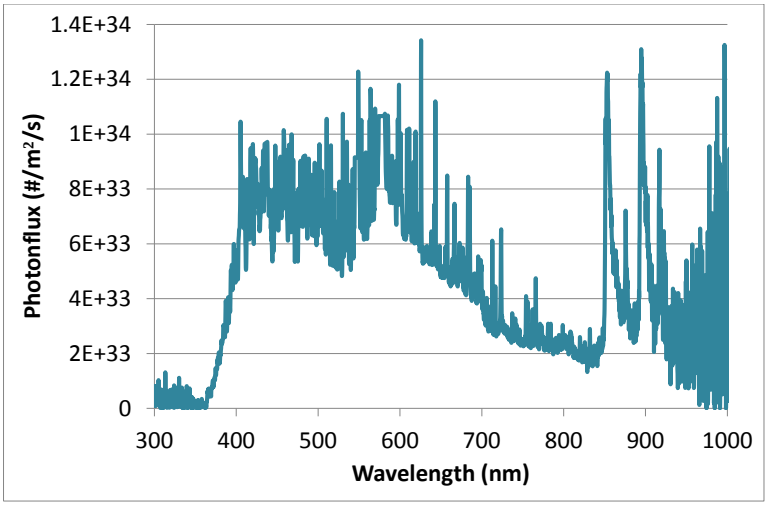

Figure E.1: The solar simulator, class B, manufactured by Steuernagel Lichtechnik (model:TCMG SOe MHL) spectrum measured by the high resolution fibre spectrometer (Ocean Optics, HR4000CG-UV-NIR).

Appendix F

PVtrace model

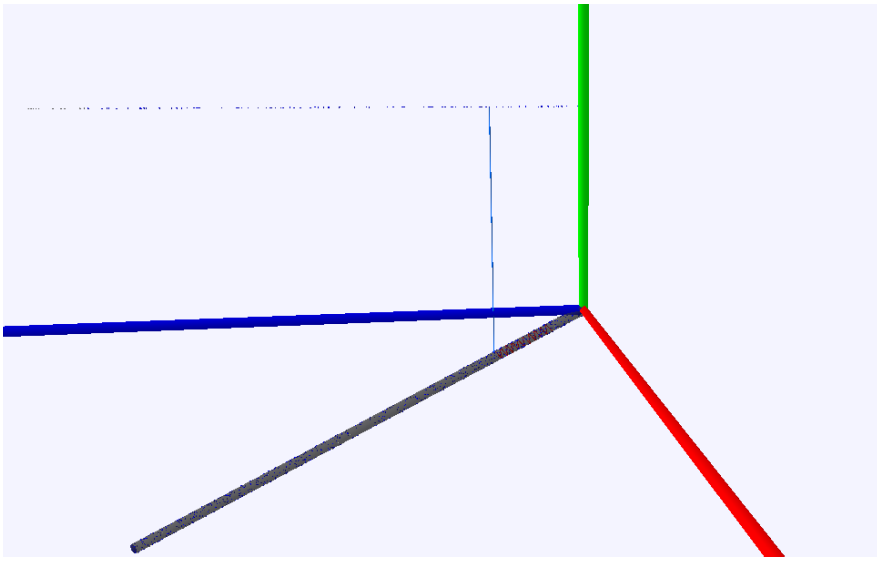

Figure F.1: Screenshot of the PVtrace simulation when modelling the direct spectrum. The fibre is placed with a certain angle to simulate the angle between position of the sun and the fibre.

Appendix G

Diffuse and Direct Spectrum Modelling

Figure G.1: Input data SMARTS for the 21st of June 2011 at 11:30

```
'Example_6:USSA_AOD=0.084'          !Card 1 Comment
1                       !Card 2 ISPR
1013.25 0. 0.               !Card 2a Pressure, altitude, height
1                       !Card 3 IATMOS
'USSA'                  !Card 3a Atmos
1                       !Card 4 IH2O
1                       !Card 5 IO3
1                       !Card 6 IGAS
370.0                   !Card 7 CO2 amount (ppm)
0                       !Card 7a ISPCTR
'S&F_URBAN'             !Card 8 Aeros (aerosol model)
0                       !Card 9 ITURB
0.084                   !Card 9a Tau500
18                      !Card 10 IALBDX
1                       !Card 10b ITILT
18 0. 0.                    !Card 10c Tilt variables (IALBDG, receiver's tilt & azimuth)
280 4000 1.0 1366.1             !Card 11 Min & max wavelengths; sun-earth distance correction; solar constant
2                       !Card 12 IPRT
280 4000 .5             !Card12a Min & max wavelengths to be printed; ideal printing step size
3                       !Card12b Number of Variables to Print
8 6 7                   !Card12c Variable codes
1                       !Card 13 ICIRC
0 2.9 0                     !Card 13a Receiver geometry (3 angles)
0                       !Card 14 ISCAN
0                       !Card 15 ILLUM
0                       !Card 16 IUV
3                       !Card 17 IMASS
2011 6 21 11.5 51.32 -0.5 0             !Card 17a Year Month Day Hour Latitude Longitude Timezone
```

Table G.1: Angle of incidence, angle between the North South axis and the sun for every hour. In the table only half a days is shown as the angle is symmetical throughout the day.

	Summer							
Time (hr)	05.30	06.30	07.30	08.30	09.30	10.30	11.30	12.30
Angle (∘)	50,76	21,90	9,19	1,58	11,88	16,91	25,52	26,55
	Winter							
Time (hr)	09.00	10.00	11.00	12.00				
Angle (∘)	42,34	42,10	52,52	51,81				

Table G.2: Optical efficiency and photons collected results for optical fibre with radius 1mm and length 10 cm modelled with PVtrace with the Direct and Diffuse spectrum of SMARTS

winter	diffuse	direct	spectrum diff	spectrum dir	diffuse	direct
time (hr)	collection (%)	collection (%)	photonflux (#)	photonflux (#)	collection (#)	collection (#)
9	0,1934013	0,0284351	1,81E+016	3,40102E+16	3,51E+015	9,671E+14
10	0,2148366	0,0507005	2,76E+016	9,65627E+16	5,92E+015	4,896E+15
11	0,2171562	0,0552213	3,21E+016	1,43074E+17	6,96E+015	7,901E+15
12	0,2124758	0,0588084	3,34E+016	1,59905E+17	7,10E+015	9,404E+15
13	0,2171562	0,0552213	3,20501E+16	1,43074E+17	6,96E+15	7,901E+15
14	0,2148366	0,0507005	2,75766E+16	9,65627E+16	5,924E+15	4,896E+15
15	0,1934013	0,0284351	1,8128E+16	3,40102E+16	3,506E+15	9,671E+14
total			1,89E+017	7,07E+017	3,99E+016	3,69E+016
summer	diffuse	direct	0,27		diffuse	direct
time (hr)	collection (%)	collection (%)	photonflux (#)	photonflux (#)	collection (#)	collection (#)
5,5	0,1925909	0,0236373	1,57E+016	2,59E+016	3,02E+015	6,12E+014
6,5	0,2126003	0,0591114	2,89E+016	1,21164E+17	6,15E+015	7,16E+015
7,5	0,2157731	0,0657886	3,74E+016	2,4506E+17	8,06E+015	1,61E+016
8,5	0,2473761	0,0760635	4,30E+016	3,75174E+17	1,06E+016	2,85E+016
9,5	0,2319086	0,0783045	4,69E+016	4,97046E+17	1,09E+016	3,89E+016
10,5	0,2238035	0,0869166	4,94E+016	5,99341E+17	1,11E+016	5,21E+016
11,5	0,237471	0,0844688	5,09464E+16	6,73549E+17	1,21E+016	5,69E+016
12,5	0,2310888	0,0742755	5,16903E+16	7,1344E+17	1,19E+016	5,30E+016
13,5	0,2310888	0,0742755	5,16903E+16	7,1344E+17	1,195E+16	5,299E+16
14,5	0,237471	0,0844688	5,09464E+16	6,73549E+17	1,21E+16	5,689E+16
15,5	0,2238035	0,0869166	4,94087E+16	5,99341E+17	1,106E+16	5,209E+16
16,5	0,2319086	0,0783045	4,68875E+16	4,97046E+17	1,087E+16	3,892E+16
17,5	0,2473761	0,0760635	4,3047E+16	3,75174E+17	1,065E+16	2,854E+16
18,5	0,2157731	0,0657886	3,73599E+16	2,4506E+17	8,061E+15	1,612E+16
19,5	0,2126003	0,0591114	2,89078E+16	1,21164E+17	6,146E+15	7,162E+15
20,5	0,1925909	0,0236373	1,5686E+16	2,5873E+16	3,021E+15	6,116E+14
total			6,48E+017	6,50E+018	1,48E+017	5,07E+017

Figure G.2: Lumogen red dye absorption compared to the silicon solar cell absorption percentage of the direct sunlight in the winter

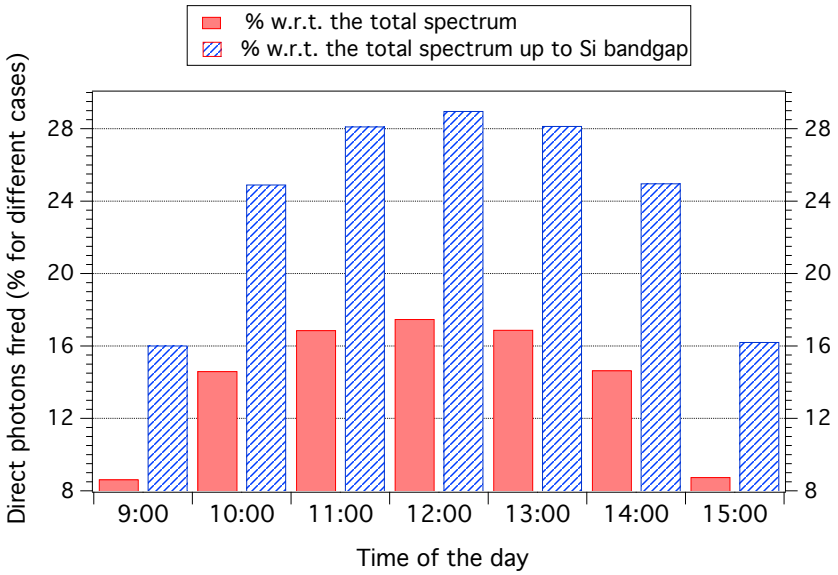

Figure G.3: Lumogen red dye absorption compared to the silicon solar cell absorption percentage of the direct sunlight in the summer

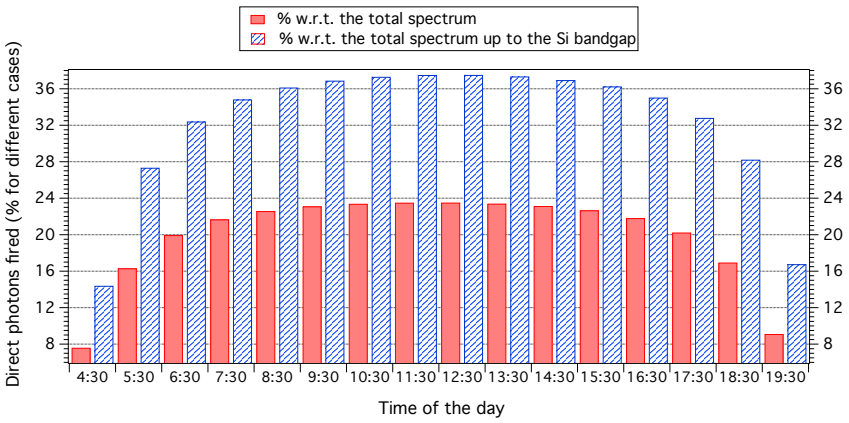

Figure G.4: Lumogen red dye absorption compared to the silicon solar cell absorption percentage of the diffuse sunlight in the winter

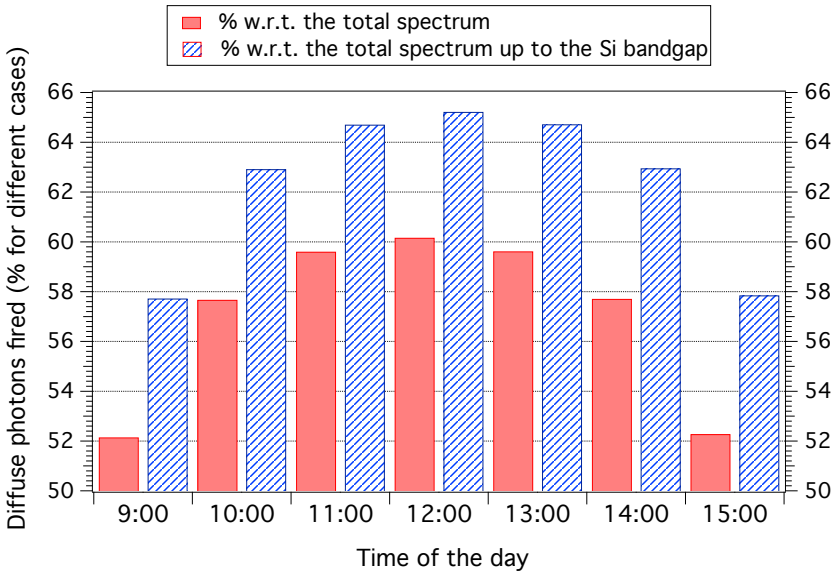

Figure G.5: Lumogen red dye absorption compared to the silicon solar cell absorption percentage of the diffuse sunlight in the summer

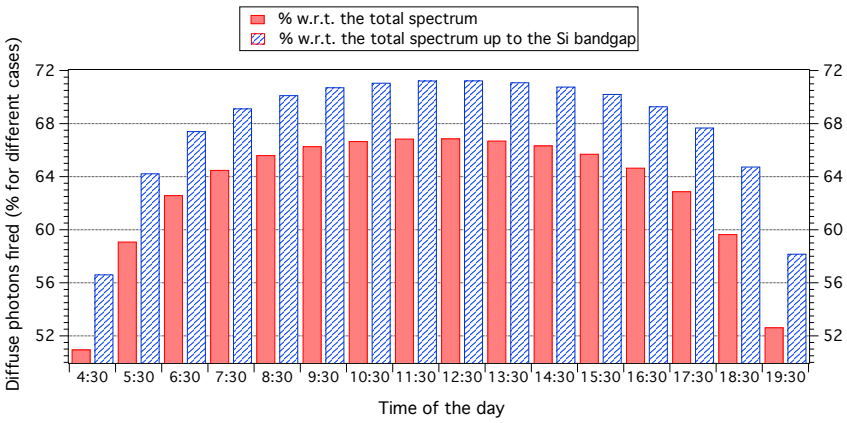

Appendix H

APE diffuse and direct spectrum London

Table H.1: :Average Photon Energy in eV of the spectra on the 21st of June 2011 and the 22nd of December 2012 in the morning with a clear sky in London. The spectra in the afternoon have the same shape as the spectra in the morning.

time (hr)	global	direct	diffuse
summer			
4.5	1.77	1.43	2.14
5.5	1.77	1.58	2.30
6.5	1.79	1.66	2.38
7.5	1.80	1.69	2.43
8.5	1.81	1.72	2.45
9.5	1.81	1.73	2.47
10.5	1.81	1.74	2.48
11.5	1.82	1.74	2.49
12.5	1.82	1.74	2.49
winter			
9	1.76	1.45	2.16
10	1.76	1.55	2.27
11	1.77	1.60	2.31
12	1.77	1.61	2.32

Bibliography

[1] I. E. Agency, ed., *Solar Energy Perspectives*. OECD/IEA, 2012.

[2] A. Jaeger-Waldau, "Photovoltaics: Status and perspectives until 2020," *Green Issue*, vol. 1, pp. 241–298, 2011.

[3] W. van Sark, K. Barnham, L. Slooff, A. Chatten, A. Buchtemann, A. Meyer, S. McCormack, R. Koole, D. Farrel, R. Bose, E. Bende, A. Burgers, T. Budel, J. Quilitz, M. Kennedy, T. Meyer, C. de Mello Donega, A. Meijerink, and D. Vanmaekelbergh, "Luminescent solar concentrators - a review of recent results," *Optical EXPRESS*, vol. 16, no. 26, 2008.

[4] K. McIntosh, N. Yamada, and B. Richards, "Theoretical comparison of cylindrical and square-planar luminescent solar concentrators," *Applied Physics B: Lasers and Optics*, vol. 88, pp. 285–290, 2007. 10.1007/s00340-007-2705-8.

[5] R. Bose, *Raytrace Simulations and Experimental Studies of Luminescent Solar Concentrators*. PhD thesis, Imperial College of London, London, UK, Oct 2010.

[6] J. Twidell and T. Weir, *Renewable Energy Resources; 2nd ed.* Abingdon: Spon, 2005.

[7] C. Gueymard, "Parameterized transmittance model for direct beam and circumsolar spectral irradiance.," *Solar Energy*, vol. 71, no. 5, pp. 325–346, 2001.

[8] C. Gueymard, "Smarts, a simple model of the atmospheric radiative transfer of sunshine: Algorithms and performance assessment.," *Professional Paper FSEC- PF-270-95. Florida Solar Energy Center, 1679 Clearlake Rd., Cocoa, FL 32922.*, 1995.

[9] W. van Sark, "Simulating performance of solar cells with spectral downshifting layers," *Thin Solid Films*, vol. 516, no. 20, pp. 6808 – 6812, 2008. <ce:title>Proceedings on Advanced Materials and Concepts for Photovoltaics EMRS 2007 Conference, Strasbourg, France</ce:title>.

[10] J. Nelson, *The Physics of Solar Cells*. London, UK: Imperial College Press, 2003.

[11] B. C. Rowan, L. R. Wilson, and B. S. Richards, "Advanced material concepts for luminescent solar concentrators," *IEEE Journal of Selected Topics in Quantum Electronics*, vol. 14 Issue:5, pp. 1312–1322, Sept 2008.

[12] B. Richards and K. McIntosh, "Ray-tracing simulations of luminescent solar concentrators containing multiple luminescent species," *Proceedings of Twentyfirst European Photovoltaic Solar Energy Conference, Munich, Germany*, pp. 185–188, 2006.

[13] J. S. Batchelder, A. H. Zewail, and T. Cole, "Luminescent solar concentrators. 1: Theory of operation and techniques for performance evaluation," *Appl. Opt.*, vol. 18, pp. 3090–3110, Sept 1979.

[14] M. J. Currie, J. K. Mapel, T. D. Heidel, S. Goffri, and M. A. Baldo, "High-efficiency organic solar concentrators for photovoltaics," *Science*, vol. 321, no. 5886, pp. 226–228, 2008.

[15] "Zemax version 12 ee, optical and illumination design software." `http://www.radiantzemax.com/en/design/`, 2012.

[16] D. Farrell, "Pvtrace – optical ray tracing for photovoltaic devices and luminescent materials." `https://github.com/danieljfarrell/pvtrace/`, 2012. [Online, accessed 15-october-2011].

[17] D. Farrell, *Characterising the Performance of Luminescent Solar Concentrators*. PhD thesis, Imperial College of London, London, UK, Aug 2008.

[18] "Industrial fiber optics website, producer of fluorescent fibres.." `http://i-fiberoptics.com/fluorescent-fiber.php`.

[19] J. C. de Mello, H. F. Wittmann, and R. H. Friend, "An improved experimental determination of external photoluminescence quantum efficiency," *Advanced Materials*, vol. 9, no. 3, pp. 230–232, 1997.

[20] A. R. Shultz, "Degradation of polymethyl methacrylate by ultraviolet light," *The Journal of Physical Chemistry*, vol. 65, no. 6, pp. 967–972, 1961.

[21] L. Wilson and B.S.Richards, "Measurement method for photoluminescence quantum yields of fluorescent organic dyes in polymethyl methacrylate for luminescent solar concentrators," *Applied optics*, vol. 48, no. 2, pp. 213–220, 2009.

[22] National Renewable Energy Laboratory (NREL), *Renewable Energy Data Book*. US: Department of Energy, 2010.

[23] BP, *BP Energy Outlook 2030*. London, UK: BP, Jan 2011.

[24] M. Born and E. Wolf, *Principles of Optics*. Cambridge, UK: Cambridge University Press, 7$^{\text{th}}$ (expanded) ed., 1999.

[25] W. Shockley and H. J. Queisser, "Detailed balance limit of efficiency of p–n junction solar cells," *Journal of Applied Physics*, vol. 32, no. 3, pp. 510–519, 1961.

[26] G. Araujo and A. Marti, "Absolute limiting efficiencies for photovoltaic energy conversion," *Solar Energy Materials and Solar Cells*, vol. 33, pp. 213–240, Nov 1994.

[27] G. Brown and J. Wu, "Third generation photovoltaics," *Laser & Photonics Reviews*, vol. 3, pp. 394–405, Jan 2009.

[28] A. Goetzberger and W. Greube, "Solar energy conversion with fluorescent collectors," *Applied Physics A: Materials Science & Processing*, vol. 14, pp. 123–139, 1977.

[29] W. H. Weber and J. Lambe, "Luminescent greenhouse collector for solar radiation," *Appl. Opt.*, vol. 15, pp. 2299–2300, Oct 1976.

[30] A. Dixon, "A Proof–of–Concept Concentrating PV/T Window Blind for Commercial Buildings," Master's thesis, Imperial College of London, London, UK, Sept 2010.

[31] G. Smestad, H. Ries, R. Winston, and E. Yablonovitch, "The thermodynamic limits of light concentrators," *Solar Energy Materials*, vol. 21, pp. 99–111, 1990.

[32] X. Peng, M. C. Schlamp, A. V. Kadavanich, and A. P. Alivisatos, "Epitaxial Growth of Highly Luminescent CdSe/CdS Core/Shell Nanocrystals with Photostability and Electronic Accessibility," *Journal of the American Chemical Society*, vol. 119, no. 30, pp. 7019–7029, 1997.

[33] X. Wang, T. Wang, X. Tian, L. Wang, W. Wu, Y. Luo, and Q. Zhang, "Europium complex doped luminescent solar concentrators with extended absorption range from UV to visible region," *Solar Energy*, vol. 85, no. 9, pp. 2179–2184, 2011.

[34] V. Fattori, M. Melucci, L. Ferrante, M. Zambianchi, I. Manet, W. Oberhauser, G. Giambastiani, M. Frediani, G. Giachi, and N. Camaioni, "Poly(lactic acid) as a transparent matrix for luminescent solar concentrators: a renewable material for a renewable energy technology," *Energy Environ. Sci.*, vol. 4, pp. 2849–2853, 2011.

[35] D. Şahin, B. Ilan, and D. F. Kelley, "Monte–Carlo simulations of light propagation in luminescent solar concentrators based on semiconductor nanoparticles," *Journal of Applied Physics*, vol. 110, no. 3, p. 033108, 2011.

[36] D. Şahin, B. Ilan, and D. F. Kelley, "Photon transport in luminescent solar concentrators based on semiconductor nanoparticles," in *Renewable Energy and the Environment*, p. JThC4, Optical Society of America, 2011.

[37] R. H. Inman, G. V. Shcherbatyuk, D. Medvedko, A. Gopinathan, and S. Ghosh, "Cylindrical luminescent solar concentrators with near–infrared quantum dots," *Opt. Express*, vol. 19, pp. 24308–24313, Nov 2011.

[38] N. C. Giebink, G. P. Wiederrecht, and M. R. Wasielewski, "Resonance–shifting to circumvent reabsorption loss in luminescent solar concentrators," *Nature Photonics*, vol. 5, pp. 694–701, Sept 2011.

[39] R. Bose, D. J. Farrell, A. J. Chatten, M. Pravettoni, A. Büchtemann, and K. W. J. Barnham, "Novel configurations of luminescent solar concentrators," *The Compiled State–of–the–Art of PV Solar Technology and Deployment*, no. JRC42252, pp. 210–214, 2007.

[40] S. Chandra, S. J. McCormack, J. Doran, M. Kennedy, and A. J. Chatten, "New concept for luminescent solar concentrators," in *Proceedings of the 25th European Photovoltaic Solar Energy Conference and Exhibition*, (Valencia, Spain), pp. 1–5, Sept 2010.

[41] R. Bose, D. Farrell, A. Chatten, M. Pravettoni, A. Buchtemann, J. Quilitz, A. Fiore, L. Manna, and K. Barnham, "Luminescent Solar Concentrators: Nanorods and Raytrace Modeling," in *Photovoltaic Specialists Conference, 2008. PVSC '08. 33rd IEEE*, (San Diego, CA), pp. 1–5, May 2008.

[42] S. T. Bailey, G. E. Lokey, M. S. Hanes, J. D. Shearer, J. B. McLafferty, G. T. Beaumont, T. T. Baseler, J. M. Layhue, D. R. Broussard, Y. Zhang, and B. P. Wittmershaus, "Optimized excitation energy transfer in a three–dye luminescent solar concentrator," *Solar Energy Materials and Solar Cells*, vol. 91, no. 1, pp. 67–75, 2007.